


國立交通大學

顯示科技研究所

碩士論文

光學結構於電致發光元件出光效率之提升



**The Enhancement of Light Extraction
Efficiency of Electroluminescent device by
Optical Structure**

研究生：林哲仁

指導教授：田仲豪 博士

中華民國九十五年七月

光學結構於電致發光元件出光效率之提升

**The Enhancement of Light Extraction
Efficiency of Electroluminescent device by
Optical Structure**

研究生: 林哲仁

Student: Che-Jen Lin

指導教授: 田仲豪

Advisor: Dr. Chung-Hao Tien

國立交通大學 電機學院

顯示科技研究所

碩士論文

A Thesis

Submitted to Institute of Electro-Optical Engineering
College of Electrical Engineering and Computer Science

National Chiao-Tung University

in Partial Fulfillment of the Requirements

for the Degree of

Master

In

Electro-Optical Engineering

June 2006

Hsin-Chu, Taiwan, Republic of China

中華民國九十五年七月

光學結構於電致發光元件出光效率之提升

碩士研究生：林哲仁

指導教授：田仲豪博士

國立交通大學 顯示科技研究所

中文摘要

近年來，由於有機發光二極體(OLED)及發光二極體(LED)等電致發光元件(Electroluminescence devices)大量應用於LCD等顯示器或照明設備上，有輕薄，可撓式(flexible)等優點，。然而，其較低的出光效率仍是一個極需解決的問題。當光源從主動層(active layer)發出時，大部分的光會侷限(trapped)在高折射率層中，導致出光效率低。且在基版(substrate)與空氣的介面上由於全反射的影響，部分的光會被反射回來，此亦為造成出光效率低的原因之一。為提升電致發光元件的出光效率，在此我們利用二維光子晶體及微透鏡陣列等光學結構達到效率增加的目的。以光子晶體與微透鏡陣列分別應用於有機發光二極體(OLED)及發光二極體(LED)，以檢視奈米與微米等級的光學結構，在電致發光元件上所能提升的效率。根據模擬結果，將二維光子晶體結構應用於有機發光二極體上可得到1.17倍的提升。以微透鏡陣列應用於發光二極體上，則可得到1.35倍的效率增加。

The Enhancement of Light Extraction Efficiency of Electroluminescent device by Optical Structure

Student: Che-Jen Lin

Advisor: Chung-Hao Tien

**Display Institute
National Chiao Tung University**

Abstract

Electroluminescent devices such as OLEDs and LEDs applied on flat panel display (ex. LCD) or lighting devices have the features of light weight and flexible. However, the low light extraction efficiency is one of the critical issues needed to be solved. When the light emitted from the active region, large portion of the light will be trapped inside the high-index layers which results in low extraction efficiency. Moreover, due to the total internal reflection effect at the interface between substrate and air, part of the light will be further reflected. As a consequence, only small portion of the emitted light will extract into the air. In order to enhance the light extraction efficiency of such electroluminescent devices, a two-dimensional photonic crystal structure and a microlens arrays are applied onto OLED and LED, respectively. An estimation of such nano and micro scale optical structures applied on electroluminescent devices is made to see how the efficiency can be increased. According to our simulation result, 117% and 135% of enhancements in PC-OLED and microlens array based LED is obtained.

Acknowledgement

In my graduate life, I am especially thankful to Professor Chung-Hao Tien, who gave me many valuable advices on my research. Prof. Tien also provides me an excellent research environment to finish my diploma.

Besides, my senior classmate, Pi-Ju Cheng, helps me a lot on my study. As for my classmates, Ming-Jing Chien, Yen-Hsing Lu, Chien-Hsiang Hung and Wei-Liang Kao, who have accompanied me for these two years and made my graduate life colorful and enjoyable. I have a lot of happy memories with them. The junior classmates, Shih-Wei Ying, Tzu-Hsiang Lan, Yuan-Jung Yao, Shun-Ting Hsiao and Cho-Chih Chen, also bring me joy and fun. Thanks for their feedbacks on my research. Paul, labmate from French, gives me a special experience of culture exchange and impressive image about France. Special thank for Jeffrey Mao and Shou-Ren Chen in ITRI for helping on fabrication part. I also appreciate the help of Paul Yang in my experimental measurement.

Finally, I would like to thank my family. Without their cultivation and support, I can't be what I am today. With their considerate care, I can focus on my research and accomplish my diploma without worrying anything. It's my pleasure to share my happiness with my family and those who ever help me.

Che-Jen Ivan Lin

July 2006

Table of Contents

Abstract (Chinese)	i
Abstract (English)	ii
Acknowledgement	iii
Table of Contents	iv
Figure Captions	vi
List of Tables	viii
Chapter 1 Introduction	1
1.1 Efficiency of OLED	1
1.2 Photonic Crystals on OLED	3
1.3 Microlens Array on Electroluminescent Devices	3
1.4 Motivation and Objective of This Thesis	4
1.5 Arrangement of This Thesis	4
Chapter 2 Theory and Simulation of PC-OLED	5
2.1 Introduction	5
2.2 Simulation of PC-OLED	6
2.2.1 Thickness of ETL	6
2.2.2 Dipole Direction	8
2.3 The Effect of PC	8
2.3.1 The Principle of Grating	9
2.3.2 Bloch Theory	10
2.3.3 Waves in Grating Structure	11
2.4 Fully Analysis of PC-OLED	17
2.4.1 Photonic-Band Diagram	18
2.4.2 Modes Distribution	20
Chapter 3 Nano-imprinting Technology	23
3.1 Introduction to Nano-imprinting Lithography	23
3.2 UV-NIL	24
3.3 Key Issues in UV-NIL	25
Chapter 4 OLED/LED with Microlens Array	29
4.1 Basic Analysis of LED	29
4.2 Introduction to Monte Carlo Method	33

4.3 Microlens Array Based LED -----	34
4.3.1 Mathematical Prediction -----	36
4.3.2 Ray-tracing Simulation Result -----	39
Chapter 5 Conclusion -----	41
5.1 Conclusion -----	41
Reference -----	43



Figure Caption

Fig. 1.1 Fig. 1.1 Flexible OLED products and LED-based display application -----	1
Fig. 1.2 The fraction of energy in each mode -----	3
Fig. 2.1 (a) schematic of PC-OLED (b) thickness and refractive index (c) period and depth of PC -----	5
Fig. 2.2 Optical model of PC-OLED -----	6
Fig. 2.3 Image dipoles induced by metal layer -----	7
Fig. 2.4 The far-field patterns with ETL (a) 80nm (b) 100nm -----	7
Fig. 2.5 Light distribution of (a) in-plane (b) vertical dipole sources -----	8
Fig. 2.6 (a) K-space presentation of outside, leaky, and guided modes, (b) modes in LED -----	10
Fig. 2.7 Illustration for Bloch theorem -----	10
Fig. 2.8 (a) Monomode slab waveguide (b) associated WVD -----	12
Fig. 2.9 (a) layered structure (b) associated WVD -----	13
Fig. 2.10 Grating-based device -----	14
Fig. 2.11 Extended WVD -----	15
Fig. 2.12 1D grating WVD -----	16
Fig. 2.13 Photonic-band diagram of 2D lattice for TE mode. (a) $n_1=2.0$ and $n_2=1.7$ and (b) $n_1=3.4$ and $n_2=1.0$ -----	18
Fig. 2.14 Extraction efficiency as a function of PC period -----	19
Fig. 2.15 Photonic-band diagram (a) TM-like (b) TE-like -----	20
Fig. 2.16 (a) schematic depicting the OLED structure and computational model. Ratio of each mode to the total emission rate as a function of the thickness of (b) ITO layer. (c) Alq3 layer -----	21
Fig. 2.17 Ratio of air modes, substrate modes, and high-index modes as a function of PC	

periods -----	22
Fig. 3.1 Imprinting with unparallism -----	26
Fig. 3.2 Imprinting with in-uniform pressure -----	26
Fig. 3.3 (a) SEM (b) AFM of fabricated PC structure -----	28
Fig. 4.1 Schematic of LED (a) LED chip (b) LED lamp -----	29
Fig. 4.2 Boundary condition at the interface between two media (a) TM (b) TE -----	30
Fig. 4.3 Transmittance as a function of incident angle θ_i -----	31
Fig. 4.4 Escape cone of a photon at a active layer -----	31
Fig. 4.5 (a) trapped-photon trajectories in flat surface chip (b) randomized photon trajectories off a textured surface -----	32
Fig. 4.6 (a) optical model of LED with microlens array (b) parameters of microlens array -----	35
Fig. 4.7 The light distribution in the active layer region and bottom of central microlens -----	36
Fig. 4.8 Illustration of calculating (a) Θ_{All} (b) calculation result -----	38
Fig. 4.9 Enhancement factor with different L and H -----	39
Fig. 4.10 Enhancement factor with different filling factors -----	40
Fig. 4.11 Filling factor (a) >50% (b) 50% -----	41
Fig. 4.12 Enhancement factor with different heights of superlens -----	41
Fig. 4.13 Enhancement factor with different coverage ratio under same curvature -----	42
Fig. 4.14 Illustration of relation between enhancement factor and (1) coverage ratio (2) curvature -----	43

List of Tables

Table 3.1 Comparison of present nano-imprinting lithography ----- 41



Chapter 1

Introduction

Recently, electroluminescent devices such as OLEDs or LEDs have taken the leading position for next generation display and illumination applications. Taking the advantages of such layered devices, FPDs or lighting products based on LEDs or OLEDs have the features such as thinner, lighter and flexible. However, owing to the low efficiency of LEDs and OLEDs, the resulting devices consume more power and have shorter lifetime. In order to overcome the problems, many approaches have been proposed for enhancing the extraction efficiency of OLEDs and LEDs. In this thesis, we focus our attention on the methods utilizing optical structures to obtain the enhancement of light extraction efficiency. On account of the limitation of acquirable fabrication source, we concentrate our research on **photonic crystal** on OLED (nano-scale) and **microlens-array** based LED (micro-scale).



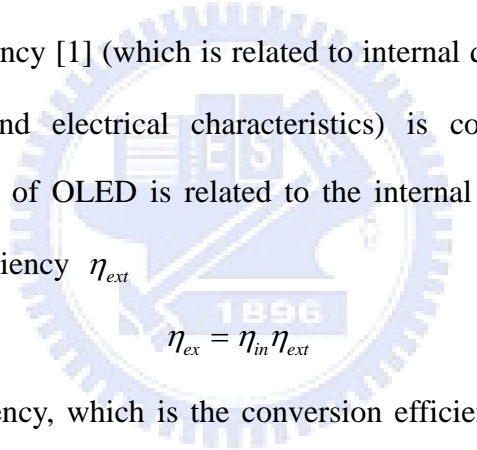
Fig. 1.1 Flexible OLED products and LED-based display application.

1.1 Efficiency of OLED

Organic light-emitting diodes (OLED) have attracted much attention in recent years on account of their potential for applications in flat panel displays and flexible

display. The OLED is a promising electronic lighting device made by combining both organic and inorganic materials, such as organic luminescent layers, organic electron-hole injection layers, a metal electrode, and a transparent ITO electrode. However, OLEDs have to be developed to meet the standards required by the industry since the overall efficiency is still low. Figure 1 shows the flexible products of OLEDs.

Various efforts have been made to improve the performance of OLEDs. The improvement of luminous efficiency of OLEDs is the key issue that must be resolved if one wants to apply such devices on display applications. Both low power consumption and long lifetime are required. To realize these requirements, the luminance-power efficiency [1] (which is related to internal quantum efficiency, light extraction efficiency and electrical characteristics) is considered. The external quantum efficiency η_{ex} of OLED is related to the internal quantum efficiency η_{in} and light extraction efficiency η_{ext}


$$\eta_{ex} = \eta_{in} \eta_{ext}$$

Internal quantum efficiency, which is the conversion efficiency of excited electrons into photons, is predominantly an intrinsic property of a material. Thus far, this has been improved by introducing multilayer structures, doping of fluorescent dyes, the improvement of carrier-injection layers and the use of phosphorescent harvester [2]. The internal quantum efficiency has been optimized such that it now approaches the theoretical limit [3~5]. Light extraction efficiency, which is defined as the proportion of photons generated inside a material that exit a device, has been estimated around 20% of internal quantum efficiency [6]. Large portion of the photons generated in the active region are waveguided inside high-index layer (~50%) and/or suffer total internal reflection (TIR) at the interface between air and glass substrate (~30%). The fraction of energy in each modes are shown in Figure 1.2.

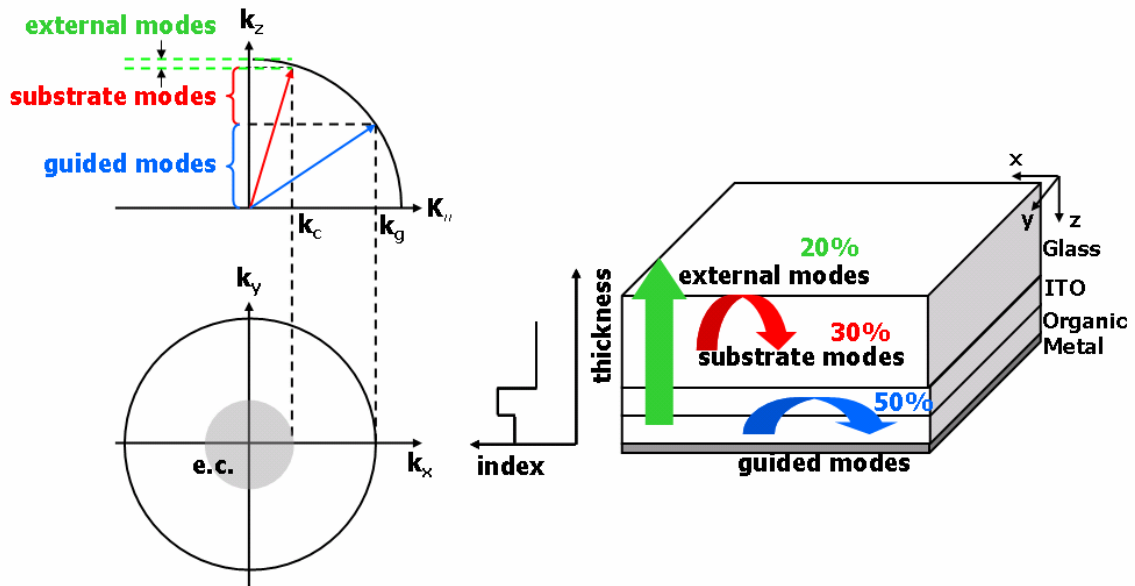


Fig. 1.2 The fraction of energy in each mode.

Therefore, in order to further improve the extraction efficiency of OLEDs, several out-coupling schemes have been implemented to overcome waveguided and TIR problems of OLED such as the incorporation of distributed Bragg reflector (DBR), mesa formation, the introduction of scattering material, the use of microlens, the insertion of low-index materials and the utilization of Bragg diffraction [2].

1.2 Photonic Crystals on OLED

Photonic crystals (PC) structure have previously used with the aim of increasing the extraction efficiency of LED [7]. Motivated by the successfully implemented of PC into LED, similar approach has also been proposed to OLED. With the introduction of PC structure into OLED, high-index guided mode, which accounts for up to 50% of total emitted energy, can be out-coupled. Significant improvement of light extraction efficiency is expected.

1.3 Microlens Array on Electroluminescent Devices

Among these methods mentioned above, the fabrication of microlens array is simple and can be applied to large area substrates [8]. The merit of microlens array on

OLED is that since this micro structure is external to the OLED devices, therefore it does not affect the operation mechanism of OLED. Furthermore, no spectral variation with viewing angle or any change on device electrical properties is observed. Such a microlens array applied on GaN LED has been used for enhancing light extraction efficiency [9]. In order to optimize the out-coupling enhancement, the geometric structure of microlens array is studied.

1.4 Motivation and Objective of This Thesis

As illustrated above, the light extraction efficiencies of both OLED and LED are so low. In recent years, several approaches have been proposed. Among these methods, we adopted the photonic crystal structure on OLEDs. The size of the patterned structure can be achieved to wavelength scale. Besides the fabrication process of PC by utilizing nano-imprinting is faster and more convenient than the conventional one. Therefore, large area PC-based OLED is proposed and discussed in this thesis.

Owing to the simple fabrication process of microlens array, microlens array can be applied on both OLED and LED to increase the extraction efficiency. To optimize the enhancement, the effects of microlens array on OLED/LED were also simulated.

1.5 Arrangement of This Thesis

The thesis is arranged as follows: the principles and the characteristic of photonic crystals structure on OLED will be described in **Chapter 2**. The simulation result will be shown in this section as well. In **Chapter 3**, the fabrication of photonic crystals structure by using nano-imprinting will be presented. The simulation result of microlens on LED will be discussed in **Chapter 4**. The conclusion of the dissertation and the future work are given in **Chapter 5**.

Chapter 2

Simulation of Photonic Crystal OLED

2.1 Introduction

In this chapter, the overview of optical properties of applying 2D photonic crystal structure into an OLED is provided. Analyses based on finite-difference time-domain (FDTD) method for the design of efficient PC-OLED is discussed. The FDTD method shows an effective way to model such complex layered OLED devices. Besides, due to the size of PC (in the wavelength scale), common raytracing method is limited for simulating the physical properties of PC. Therefore, the FDTD method is employed. Similar research studied by Yong-Jae Lee *et al.* is depicted in Fig. 2.1[10~11].

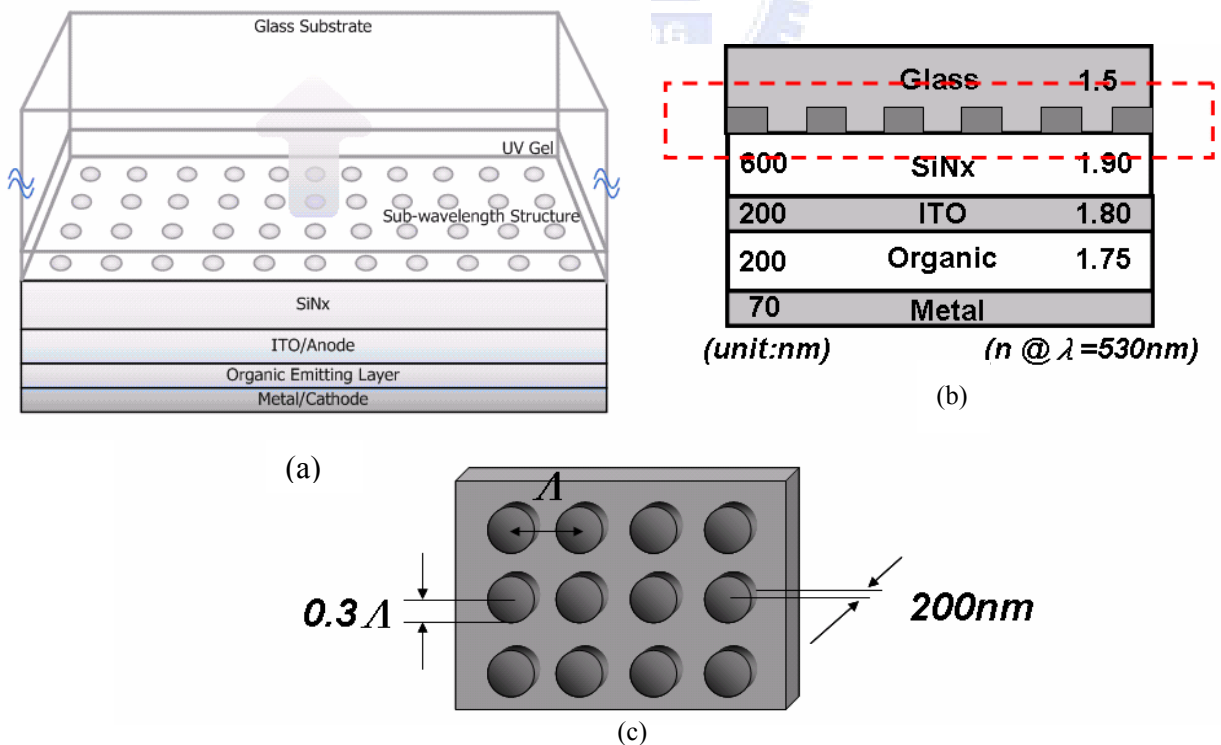


Fig. 2.1 (a) schematic of PC-OLED (b) thickness and refractive index (c) period and depth of PC

2.2 Simulation of PC-OLED

The point differs our model from Lee's is that one UV sensitive layer was added for patterning PC structure. Figure 2.2 shows the schematic of our optical model. The thickness and refraction index of each layer are also shown.

	Glass	1.5
	UV	1.5
600	SiNx	1.90
200	ITO	1.80
200	Organic	1.75
70	Metal	

(unit:nm) (n @ λ =530nm)

Fig. 2.2 Optical model of PC-OLED

In order to increase the extraction efficiency, each part of PC-OLED should be considered. Among various mechanisms, the feature of the PC layer and the thickness of electron-transport layer (ETL) are the most important and the corresponding analysis is needed.

2.2.1 Thickness of ETL

Due to the microcavity effect [10~11], the thickness of ETL plays a crucial role in extraction efficiency. With the consideration of image effect in the metal layer, thickness of ETL is controlled to satisfy the constructive interference condition.

$$\frac{\lambda}{4n_{ETL}}$$

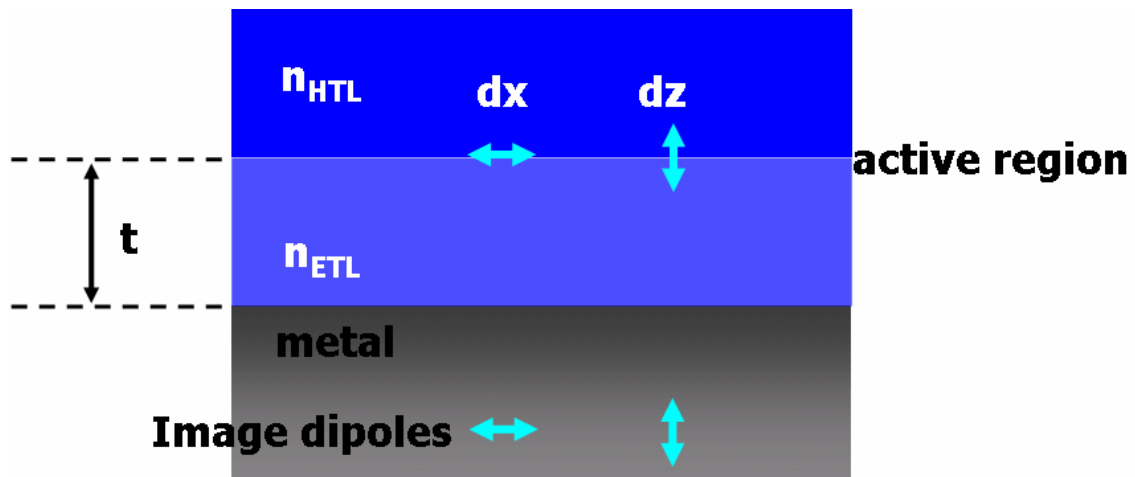


Fig 2.3 Image dipoles induced by metal layer.

As depicted in Figure 2.3, image dipoles will be induced by metal layer. Constructive interference among these dipoles is expected. Therefore we varied the thickness of ETL to see how the extraction efficiency is influenced. The simulation result with two different thicknesses is shown in Figure 2.4. The far-field pattern (intensity) within 40 degree was improved when the thickness changed from 100nm to 80nm. (The critical angle between glass ($n=1.5$) substrate and air is 40 degree.) The contour shown in Figure 2.4 depicts the viewing angle and the dark circle is the extraction cone for glass/air interface.

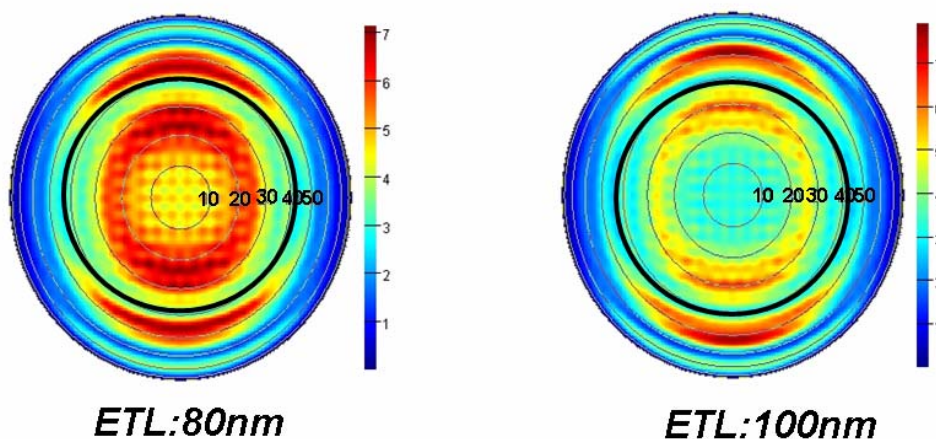


Fig 2.4 The far-field patterns with ETL (a) 80nm (b) 100nm

The analyses and simulation done above are based on the assumption that only an in-plane dipole is placed inside the OLED structure. The metal shown in Figure 2.3 is assumed as a perfect metal. Therefore there is no additional phase term in the constructive interference equation. If a realistic metal is considered, there should be an additional phase term in the equation [12].

In the constructive interference analysis, we only consider the interference between the in-plane dipole and the induced one. However, in the simulation of dipoles as the emitting source in OLED active region, dipoles are randomly distributed. This randomized behavior has increased the difficulty of analyzing the interference effect among dipoles. The research that light emission by multipole sources in thin layers has been done by Lukosz [13]. The further analysis of such effect can be studied by this reference.

2.2.2 Dipole Direction

There are two layers in the organic layer, electron-transport layer (ETL) and hole-transport layer (HTL). When the voltage applied on cathode (ITO) and anode (metal), the holes and electrons will pass through HTL and ETL, respectively. The photon will be then generated because of the combination of hole and electron. The mechanism that the source emitted from active region can be modeled as dipoles [10~11]. Light sources, radiative excitons in active layer are assumed as vertical and in-plane dipoles. Compared with the vertical dipoles, the light emitted by in-plane ones is more likely to escape into air because of the direction of dipoles. Figure 2.5 (a) and Fig.2.5 (b) show the electric fields emitted from dipoles in conventional OLED with different orientations. In both cases, portion of the electric field is confined in ITO/organic layers, which results in the low extraction efficiency. To resolve this problem, PC structure is introduced into OLED to extract the confined light in the

high-index layer.

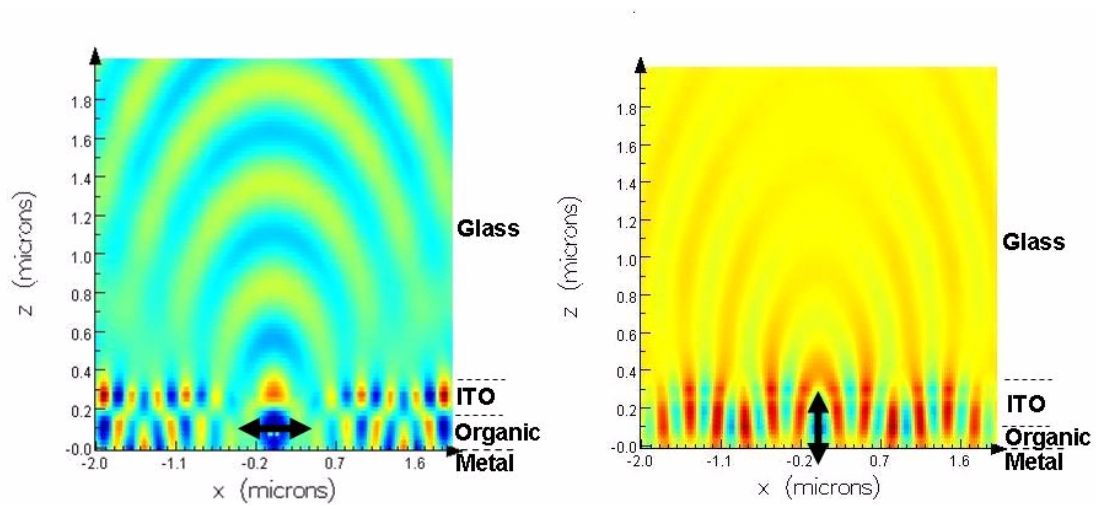


Fig. 2.5 Light distribution of (a) in-plane (b) vertical dipole sources

2.3 The effect of PC

Such 2D periodically corrugated structures can be regarded as gratings or photonic crystal structure. Here in this thesis, the analyses based on regarding such 2D periodically corrugated structure as grating and photonic crystal are both considered and discussed in the following sub-sections.

2.3.1 The Principles of Gratings

To increase the total amount of the extracted light from organic light-emitting diodes, we use corrugation at the interface to couple the guided light to running waves that propagate outside the structure. The use of grating to extract guided light has been extensively treated in the domain of integrated optics. Although most of the reported studies deal with gratings with a periodicity along one direction, it is

necessary to consider crossed gratings, which exhibit periodicity along two orthogonal directions, to couple out the total guided mode power regardless of the azimuthal direction of the guided mode. In principle, corrugation structure can be applied to any type of microcavity of supporting trapped or guided modes, we limit our analyses to planar structures. In this section, we use grating theory to analyze the physical mechanism of such devices.

The grating-assisted LED for obtaining higher brightness based on a resonant cavity containing 2D periodically corrugated layers was studied [14]. In Danaë *et al.*'s research, using wave-vector diagram (WVD) for analyzing grating structures in layered devices with was reported. We followed the same analysis approach on our model.

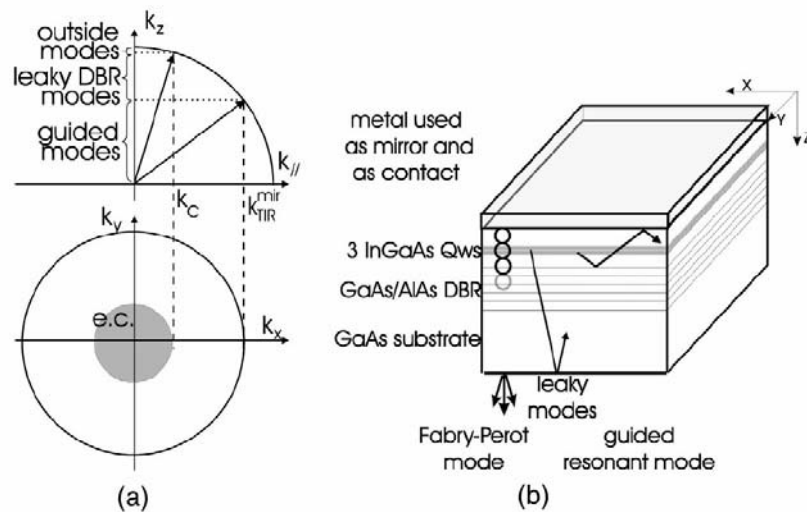


Fig. 2.6 (a) k-space presentation of outside, leaky, and guided modes, (b) modes in LED

2.3.2 Bloch Theory

If one wave propagates in the 1-D periodic structure, the adjacent fields differ with one phase term. This is so called **Bloch theorem**.

$$\varphi(x + d) = e^{-j\kappa_x d} \varphi(x)$$

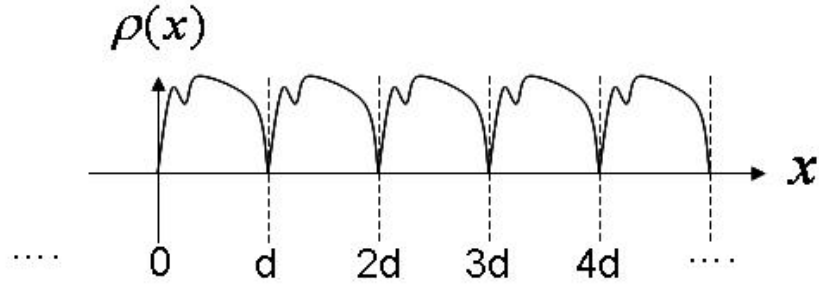


Fig. 2.7 Illustration for Bloch theorem.

assuming that:

$$\begin{aligned} \varphi(x) &= e^{-j\kappa_x x} \rho(x) \\ \rho(x) &= \rho(x + d) \end{aligned}$$

where the $\rho(x)$ is a periodic function. Substituting the second equation into the first one, we can get that

$$\begin{aligned} \varphi(x + d) &= e^{-j\kappa_x (x+d)} \rho(x + d) \\ &= e^{-j\kappa_x x} e^{-j\kappa_x d} \rho(x) \\ &= \varphi(x) e^{-j\kappa_x d} \end{aligned}$$

Since $\rho(x)$ is a periodic function, it can be expanded by Fourier series.

$$\begin{aligned} \rho(x) &= \sum_{n=-\infty}^{\infty} P_n e^{-jn \frac{2\pi}{d} x} \\ \varphi(x) &= \sum_{n=-\infty}^{\infty} P_n e^{-j\kappa_x x} e^{-jn \frac{2\pi}{d} x} \\ &= \sum_{n=-\infty}^{\infty} P_n e^{-j(\kappa_x + n \frac{2\pi}{d}) x} \end{aligned}$$

where P_n denotes the field amplitude. We define that

$$\kappa_{xn} = \kappa_x + n \frac{2\pi}{d} \quad n: \text{space harmonic}$$

The mathematical derivation for Bloch theorem done above is basic for WVD.

2.3.3 Waves in Grating Structure

In this section, the physical insight of the radiation from a source located in a periodic structure supporting guided modes is presented. As presented by Zengerle [15~17], the propagation of light into grating structure can be interpreted by wave vector diagram (WVD). In this diagram, the associated guided modes are plotted on the \mathbf{K} space. For simplicity, assuming that a single-mode supporting layer is coated on a glass substrate. The associated schematic and wave vector diagram are depicted in Figure 2.8.

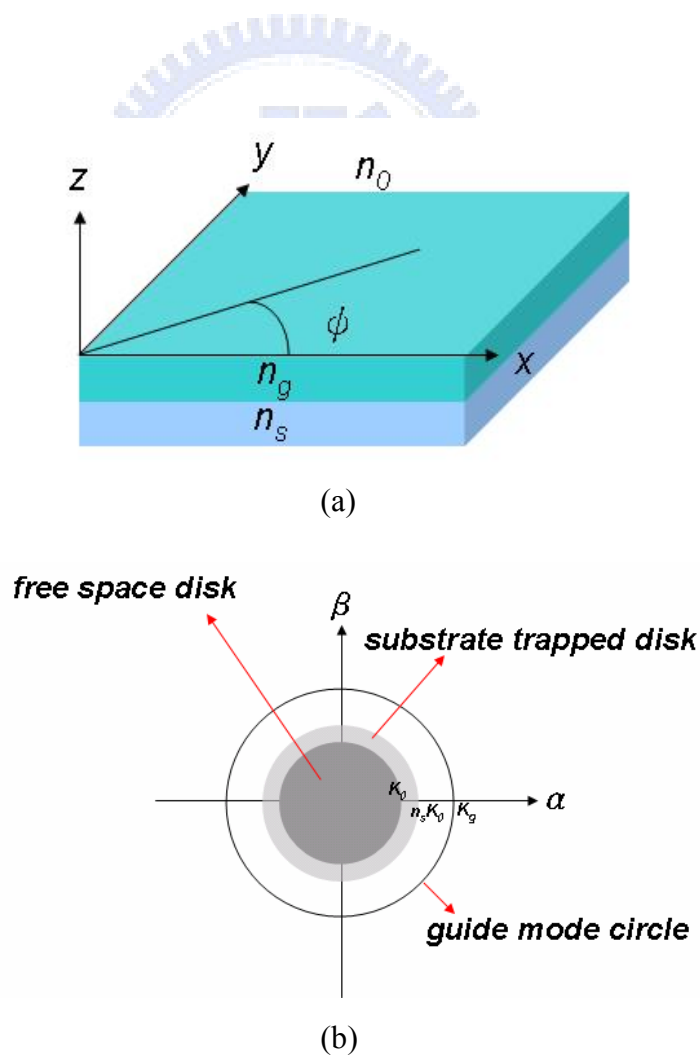


Fig. 2.8 (a) Monomode slab waveguide (b) associated WVD

Supposed that $n_g > n_s > n_0$, therefore the light will be guided and/or trapped inside this layer device. Such waveguide phenomenon can be easily understood by using WVD. According to the associated WVD, since k_g lies outside of both free space disk and substrate trapped disk, it shows no chance that wave inside layer n_g would escape.

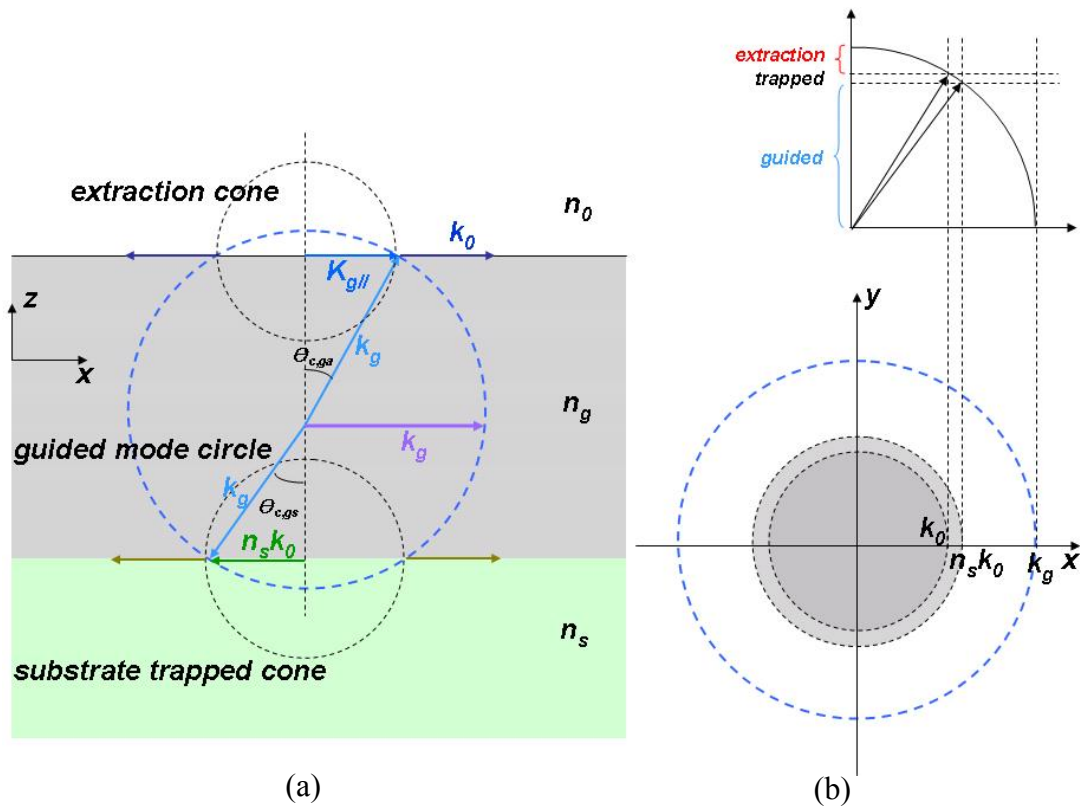


Fig. 2.9 (a) layered structure (b) associated WVD

Figure 2.9 shows the wave vectors inside a layered structure. When the wave incidents upon the interface n_0/n_g with an angle larger than the critical, the light

will be total internal reflected. According to the boundary condition, the wave vector on the boundary should be equal to each other.

$$k_g \sin \theta_{c,ga} = k_{g//} = k_0$$

The light will be reflected as long as the $k_{g//}$ larger than k_0 . On the other hand, same effect applies for the interface n_g/n_s when $k_{g//} > n_s k_0$. Therefore, we plot these two cones as disks on the right side shown in Figure 2.9(b). It can be regarded as a top view of these two cones. As the $k_{g//}$ lies inside the darker gray circle, waves would run out of this device (running wave). As for the $k_{g//}$ lies in the lighter gray region, the light will be reflected at the n_0/n_g interface but penetrating into substrate (trapped mode). Otherwise the light becomes fundamental mode guided inside the middle layer.

In order to enhance the light extraction from such kind of devices, corrugations on the surface is the most intuitive way to achieve this goal. Here, a 2D periodically corrugated structure is used to couple out the guided mode into running waves. We suppose that the period in x and y directions are d_x and d_y , respectively. (Figure 2.10)

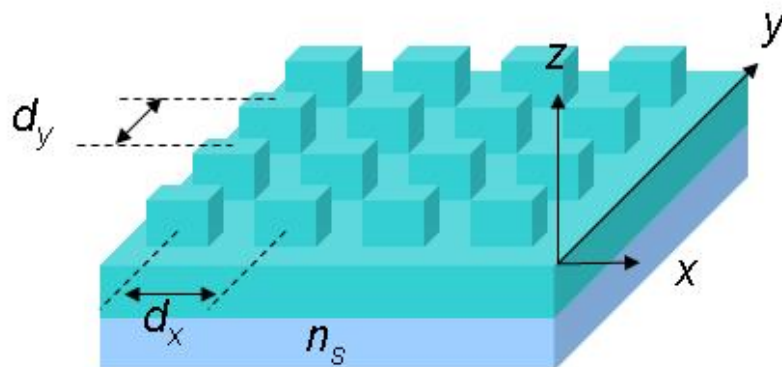


Fig. 2.10 Grating-based device

To extract the guided mode, a 2D orthogonal periodic structure is introduced on the surface. For any azimuthal angle, guided waves can be coupled through the grating since it is modulated in two directions. Assume that a wave inside the middle layer is

$$k = k_x \hat{x} + k_y \hat{y} + k_z \hat{z} = k_p + k_z \hat{z}$$

For the guided mode, $|k_p| = |k_g|$. Due to the guided mode circle never intercepts with the darker gray disk, there is no chance to extract the guided waves (see Figure 2.9(b)). However, the interception can be achieved if the surface is modulated periodically. Any wave vector k_p can be coupled to running waves through the grating based on Bloch theory. As discussed in section 2.3.2, waves extend to many space harmonics inside such a grating structure. Therefore,

$$k_p^{m,n} = kp + mG_x \hat{x} + nG_y \hat{y}$$

$$G_x = \frac{2\pi}{d_x}, G_y = \frac{2\pi}{d_y}$$

where we choose that d_x and d_y are smaller than the wavelength of radiation (sub-wavelength scale grating) and \mathbf{m} and \mathbf{n} are integers. The wave vector extends to its harmonic terms in both x and y directions. The harmonic terms implies the duplication of the disks in x and y directions with the period of G_x and G_y , respectively. As you can see from Figure 2.11, the guided circle now intercepts with the first orders duplicated disks. In other words, the guided waves now are coupled to the running waves. To make coupling effect addressed simply, we illustrate it by using one-dimension grating structure instead of the 2-D one.

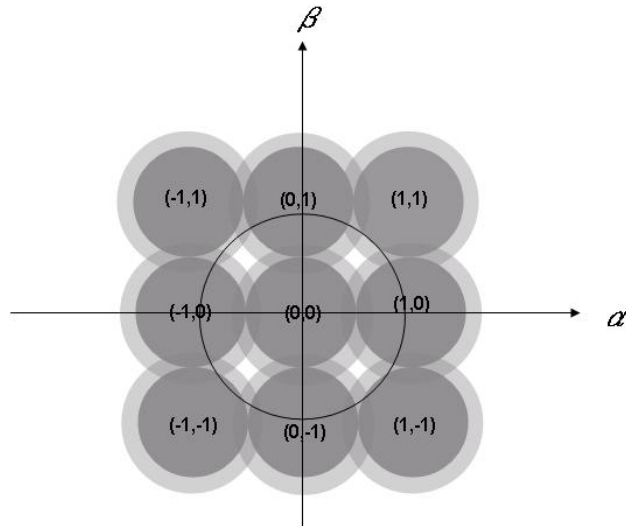


Fig. 2.11 Extended WVD

From Figure 2.12, we know that

$$k_g = k_{gx} + k_{gy}$$

where k_g is decomposed into two orthogonal terms. Assume that this 1-D grating is in x direction, k_{gx} will be modulated into harmonic terms. Since part of the guided circle overlaps with the (1,0) duplication disk, coupling takes place (solid line part).

$$\begin{aligned}
 k'_g &= k_g + mG_x \\
 &= k_{gx} + k_{gy} + mG_x \\
 &= (k_{gx} - G_x) + k_{gy} \\
 &= -k_{dx} + k_{gy} \\
 &= k_d
 \end{aligned}$$

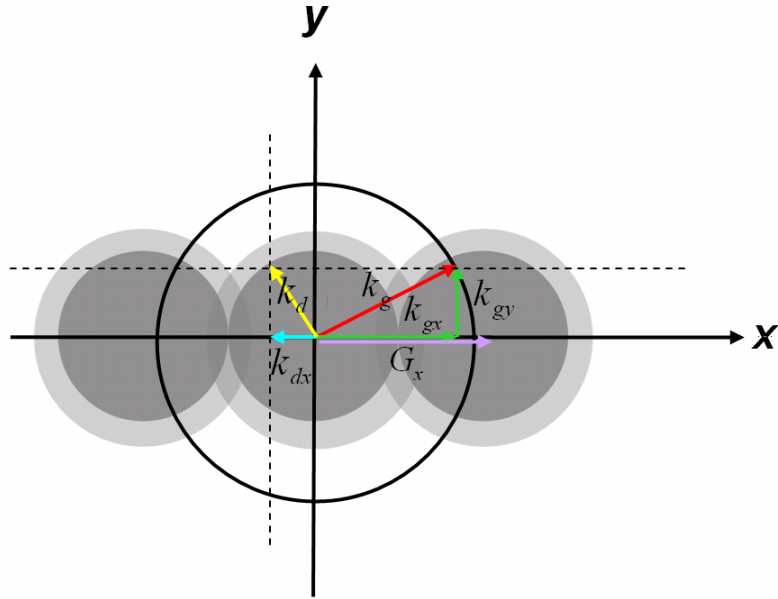


Fig 2.12 1D grating WVD

2.4 Fully Analysis of PC-OLED

The analysis above provides a general concept how this 2D periodically grating structure enhances the light extraction efficiency of OLED. However, this analysis based on regarding such structure as grating does not reveal a fully characteristics of PC-OLED. In order to have a complete understanding, an analysis based on photonic-band diagram (dispersion relation) is introduced. Before proceeding, a brief introduction of photonic-band diagram is presented as followed

Figure 2.13 (a) shows the photonic-band diagram [2]. The relative coordinates denote the wave vector (x) and normalized frequency (y), respectively. The inverse lattice diagram of PC in k -space is depicted in Figure 2.13 (c). Physically, the gray rectangle region is symmetrically equivalent to whole k -space [18]. This rectangle is composed of 8 triangles. One triangle is equivalent to another. Therefore, we only consider triangle Γ MX enclosed by points Γ , M and X as shown in Figure 2.13 (c). Any point lies on triangle Γ MX indicates one wave vector. The x -coordinate in Figure

3.13 (a) represents the wave vectors lying on the triangle with the sequence Γ , A, M, B, X and Γ .

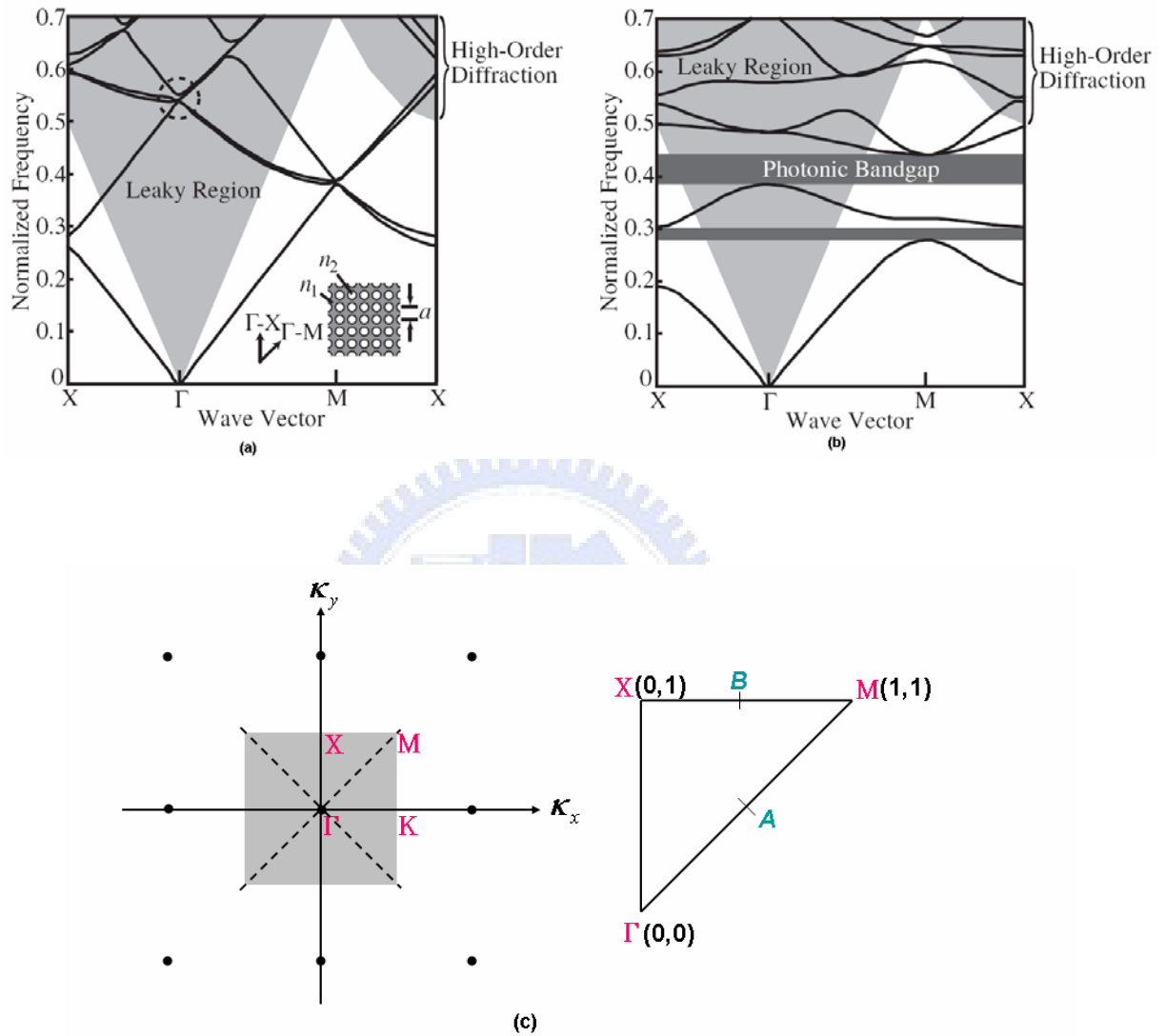


Fig. 2.13 Photonic-band diagram of 2D lattice for TE mode. The radius of the circular lattice point is set to $0.4a$ (a is period of PC); n_1 and n_2 are the refractive indices of the PC. The leaky region is calculated using the dispersion curve in air: (a) $n_1=2.0$ and $n_2=1.7$ and (b) $n_1=3.4$ and $n_2=1.0$

High index difference of PC results in the formation of photonic bandgap (PBG) in which no light can propagate, as shown in Figure 2.13 (b). The device should be designed that the waveguided mode falls within the PBG. Therefore, light-extraction

efficiency can be improved. If PC-OLED is designed as the case in Figure 2.13 (a), which the PBG is not opened, waveguided light will not be coupled into air mode. As a consequence, low extraction efficiency is obtained.

2.4.1 Photonic-band Diagram

Our simulation results are shown in Figure 2.14 and Figure 2.15. In Figure 2.14. The extraction efficiency is calculated as a function of PC period under different PC depths. When the thickness of PC layer is 250nm, higher extraction efficiency is obtained. This is due to microcavity effect. Based on our model, 1.17X enhancement can be achieved as the period of PC is 560nm.

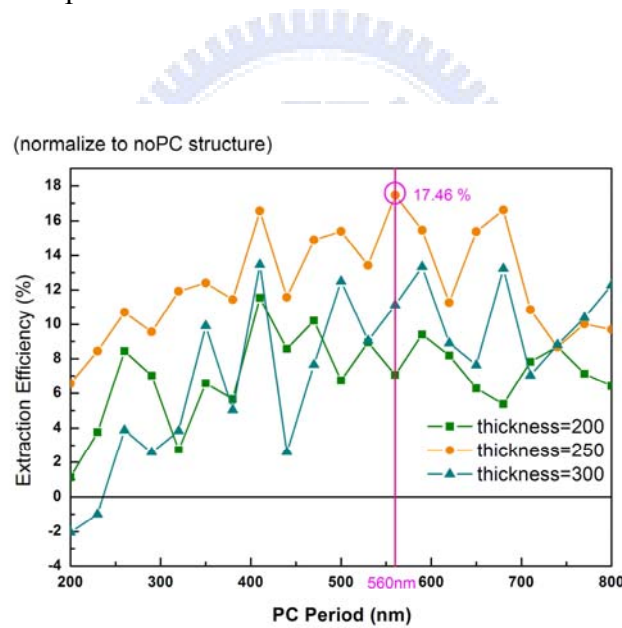


Fig. 2.14 Extraction efficiency as a function of PC period

Figure 2.15 (a) and (b) show the photonic-band diagrams with TM-like and TE-like, respectively. The plane wave expansion method is applied to calculate the photonic-band diagrams. As addressed in the previous subsection, the photonic-band diagram is expected having an open band (PBG) such that enhancement is achieved as the waveguided mode falls in PBG region. However, in our model the index difference is small. Therefore, no open band is observed in the simulation model.

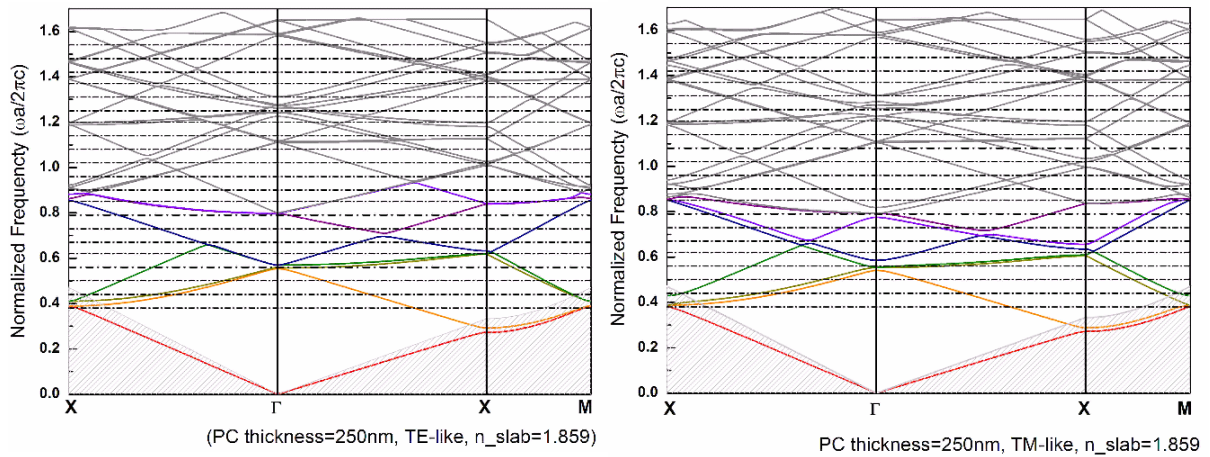


Fig. 2.15 Photonic-band diagram (a) TM-like (b) TE-like

2.4.2 Modes distribution

According to the previous research done by Chutinan *et al.*, a theoretical analysis on light extraction efficiency of a conventional OLED utilized both a numerical method (FDTD) and analytic method (mode expansion) is reported [19]. By changing the thickness of ITO or organic layer in OLED, the percentage in each mode can be re-distributed. Figure 2.16 (a) shows the schematic of OLED and computational model [19]. The modes distribution of OLED with the related thickness of ITO and Alq3 are shown in Figure 2.16 (b) and 2.16 (c), respectively. The ratios change as the layer thicknesses are varied owing to the interference effects and the generation of waveguided modes. The percentage of light in the air mode is less than 30%, whereas the waveguided mode (more than 40%) has largest proportion. This suggests that the most effective way to improve the light extraction efficiency is to couple out the waveguided mode into air mode.

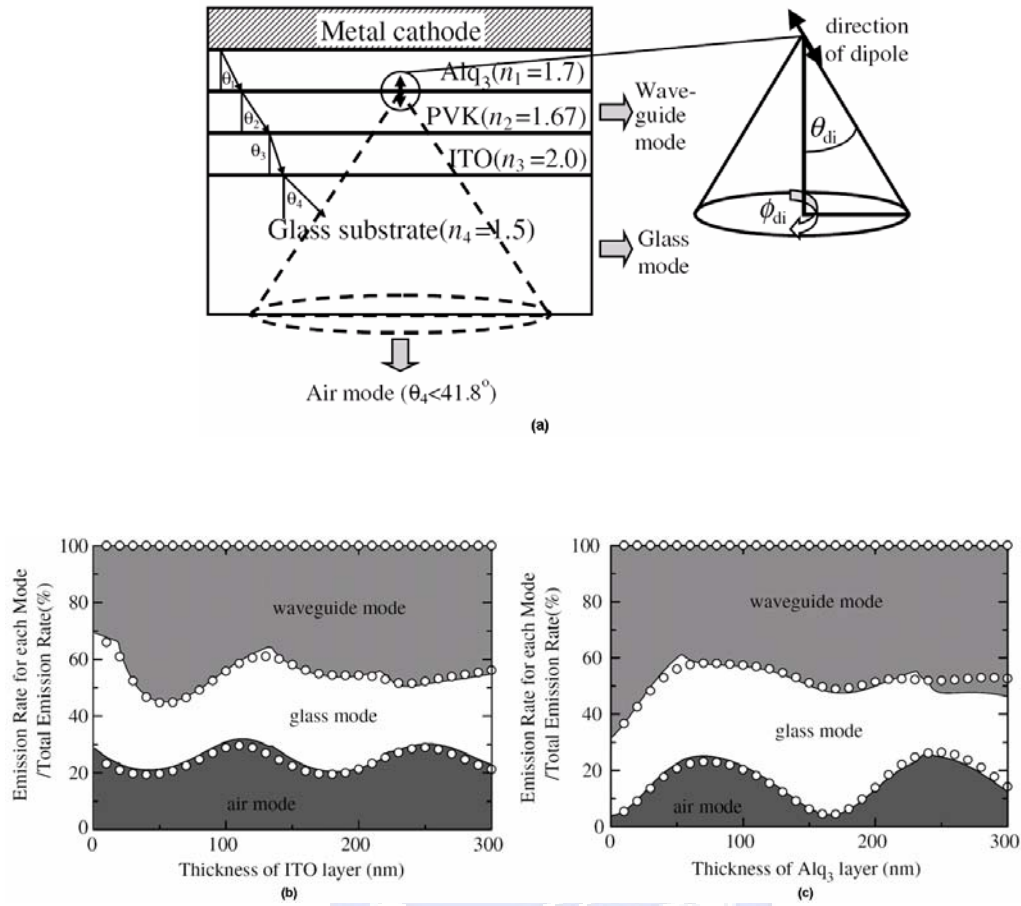


Fig. 2.16 (a) Schematic depicting the OLED structure and computational model. Ratio of the emission rate of air modes, glass modes, and waveguided modes to the total emission rate as a function of the thickness of (b) ITO layer. (c) Alq₃ layer. [19]

In order to achieve the improvement of light extraction efficiency through coupling the waveguided mode into air mode, a photonic crystal structure is introduced. As addressed previously, the high-index guided mode in OLED is coupled through the photonic crystal structure. As a consequence, light-extraction efficiency is enhanced owing to the mode-redistribution. Higher ratio in air mode was obtained coupled from high-index guided mode. Our simulation results are shown in Figure 2.17 with modes ratio as a function of PC periods with depth of 250nm.

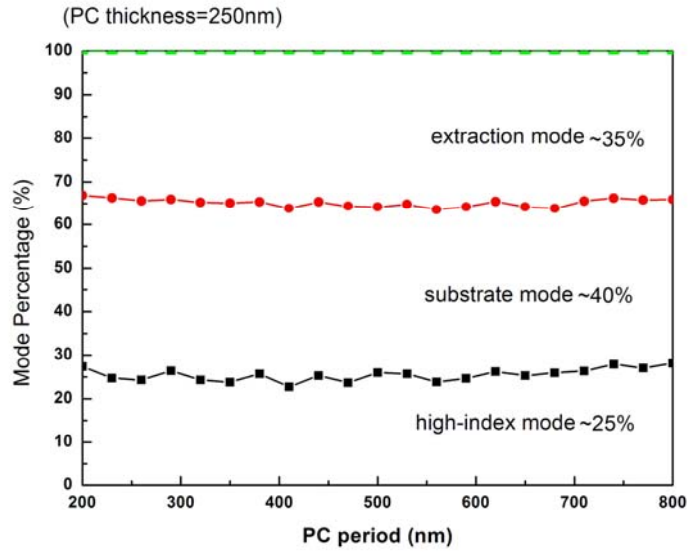


Fig. 2.17 Ratio of air modes, substrate modes (glass mode), and high-index modes (waveguided modes) as a function of PC periods.

As depicted from the figures shown above, the ratio in waveguided mode is decreased to 25%. Both air mode and substrate mode are increased. The decrease in waveguided mode results in the increase of both air mode and substrate mode. Even though the air mode is enhanced, large portion of light exists in substrate mode. This is due to the poor index difference of PC layer. Further enhancement can be obtained if the index difference increases.

Chapter 3

Nano-imprinting Technology

3.1 Introduction to Nano-imprinting Lithography (NIL) [20~21]

Owing to the advantages of high-throughput, nanometer scale resolution and low cost, nano-imprinting technology has become one of the best candidates for the next generation lithography. Since nano-imprinting technology is not limited to the diffraction limit, nano scale size structure can be realized.

The study of nano-imprinting technology started from Professor Stephen Y. Chou's paper published in 1995. Originated from the concept of imprinting, one nano-scale patterned mold was imprinted on a photoresist-coated silicon substrate by using mechanical force under high temperature and high pressure. Due to the resolution size of the mold directly reflects the patterned size, it has no limitation on the wavelength of exposure light. According to some papers, now the line width below 10 nanometers can be achieved by such technology.

Recent nano-imprinting technology can be categorized into three main streams:

- i. Hot Embossing Nanoimprint Lithography, HE-NIL
- ii. UV-Cured Nanoimprint Lithography, UV-NIL
- iii. Soft Lithography

Under high temperature and high pressure, large area nanometer scale structure can be achieved with HE-NIL. However, the thermoplastic photoresist will encounter phase change during the cooling process which would result in relaxation after de-embossing the mold. Therefore, low temperature and low pressure nano-imprinting

lithography was proposed and developed to solve this problem. For UV-NIL, such a nanometer scale structure can be done under room temperature with UV exposure. Soft lithography finished the imprinting process with a flexible mold. Since our sub-wavelength grating structure is fabricated by using UV-NIL, we will focus our attention on this technology.

Table 3.1 Comparison of present nano-imprinting lithography

	HE-NIL	UV-NIL	Soft Lithography
material of mold	hard	hard \ transparent	soft
cost of mold	high	high	low
photoresist	thermoplastic	low viscosity polymer	low viscosity liquid
structured mechanism	high T, high P	room T, UV light hardened	self-assembly monolayer
imprint force requirement	high	middle	low
imprinted area	large	middle	large
accuracy requirement	middle	high	low
yield rate	high	middle	low

3.2 UV-NIL

Same as HE-NIL, one patterned mold is prepared in advance. Because of the exposure process, the material of mold must be transparent to UV light. (Silicon is preferred) After coating the silicon substrate with low viscosity and UV sensitive

photoresist, the mold is aligned with the substrate. Mold is then embossed into photoresist layer and UV exposure is conducted right after. The purpose of UV exposure process is to make the photoresist cross-linked and hardened. Followed is de-embossing the mold.

3.3 Key Issues in UV-NIL

In order to transform the nano-scale pattern from the mold, some key issues during the process must be taken into consideration.

To uniformly transfer the nanometer scale pattern on the mold to the coating layer on substrate, the overall imprinting depth must be even, namely, the **parallelism** between mold and substrate should be highly attained and the entire pressure upon the substrate ought to be **uniform**.

Worse parallelism would result in unequal patterned depth and the nano-scale structure may not be parallel to the substrate. Some photoresist may fail to be etched over clearly in the later process because of this situation, which finally brings failure to the resulting sample. As long as the parallelism is not achieved to certain level, when the imprinting area increases, the imprinting process would fail due to some area of the transferring material (photoresist) miss the contact with the mold. To be worse situation, this may cause damage to mold and substrate. In addition to parallelism, the uniformity of the pressure distributed on sample plays an important role as well. When the pressure is not evenly imposed on sample, the resulting transferred structure may not meet the original design.

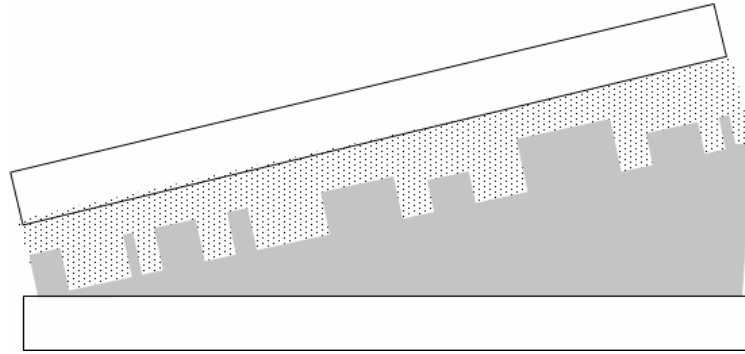


Fig. 3.1 Imprinting with unparallelism.

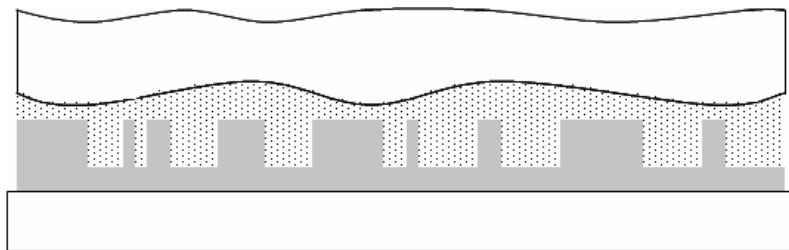


Fig. 3.2 Imprinting with in-uniform pressure.

After imprinting the pattern on photoresist, the last procedure is to de-embossing the mold. Whether the resulting sample is completely and successfully imprinted depends on this de-embossing process. If this step fails, the nano-scale structure will be deformed. Since the structure is made of polymer, the interaction between mold and polymer influences the de-embossing procedure. In general, there are two modes result in failed de-embossing. The first one is physical mode. The nano-scale structure is interlocked because of the shrinkage of polymer or the poor parallelism between mold and substrate. The other is chemical mode. The chemical bonds between mold and polymer procure viscosity. This viscosity generates difficulty on de-embossing as well. However, with the methods of plasma deposition or polymer self-assembly to coat a anti-sticking layer (several nanometers) on the mold, improvement can be achieved.

Usually the nano-scale size molds are fabricated by using E-beam lithography (EBL). The primary advantage of EBL is that the designed pattern can be obtained without mask. Moreover, the resolution is high below 10 nm. The only drawback of EBL is that the cost is high and the processing speed is slow. This yield rate is not adaptive for commercial purpose. Facing the large imprinting area in the future, the cost and yield rate still can not afford the demand. The life time of anti-sticking layer influences that of mold. Unless special mold or polymer is used, otherwise Si-based or metal mold would stick to polymer. In fact, the anti-sticking layer will be chipped off at last and mold becomes no anti-sticking function which leads to shorten the life time of mold.

The development of photoresist is also important in the nano-imprinting technology. The photoresist should have the characteristic that can be easily filled into the nano-scale structure. Appropriate fluidness should be required. Moreover, after forming, the stability, shrinkage and the spongy characteristic of photoresist should be considered as well. Generally, the resulting samples made of low viscosity material are easy to be formed and the fabrication conditions, temperature and pressure, are lower. However, the stability and the strength of such samples are poor. On the other hand, higher viscosity leads to stable structure but hard to form. Our samples are sponsored by ITRI. Thanks to ITRI's great developments on NIL, we can conduct our experiment favoringly.

The fabrication process of grating-based OLED by NIL is depicted as follows. Firstly, UV-sensitive photoresist was coated on the glass substrate. After aligning the mold with the substrate, the photoresist layer was embossed with the mold and then illuminated by UV light (320~380 nm) with the exposure time around 10 seconds to make the photoresist cross-linked and hardened. Finally, the residual photoresist on

substrate was etched after de-embossing. The grating structure fabrication was conducted under room temperature and low pressure. The total area of the resulting sample is $2 \times 2 \text{ mm}^2$. The top SEM view of grating structure and the patterned size are shown in Figure 3.3 (a) and 3.3 (b), respectively.

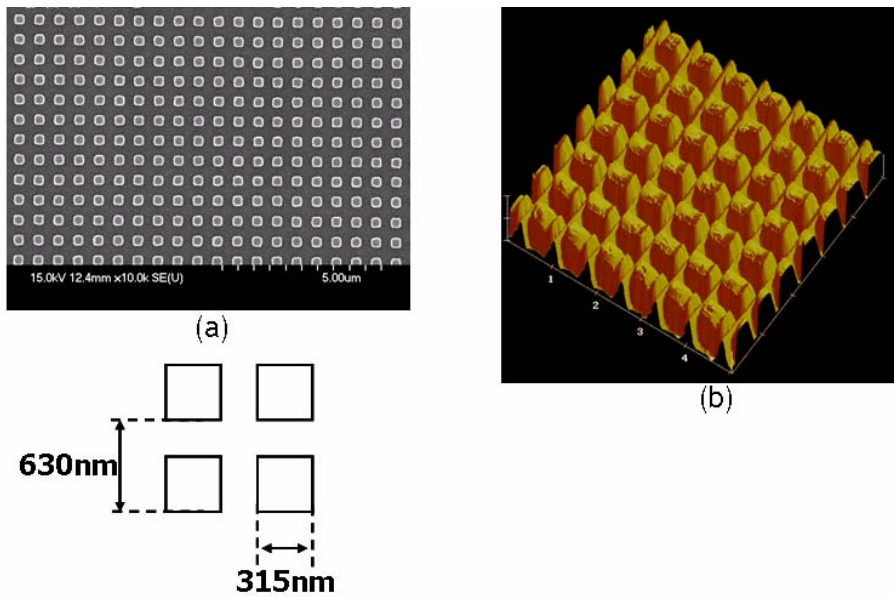


Fig. 3.3 (a) SEM (b) AFM of fabricated PC structure

Chapter 4

OLED/LED with Mircolens Arrays

4.1 Basic analysis of LED

Figure 4.1(a) shows a typical LED structure. Photons generated in the active region will incident upon the chip walls. Otherwise the photons will be absorbed internally. A conventional LED lamp is also shown in Figure 4.1(b).

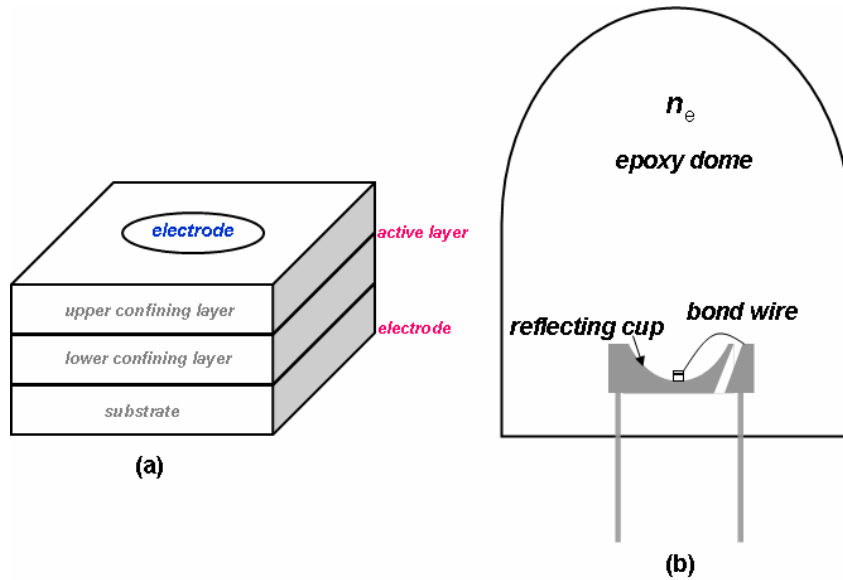


Fig 4.1 Schematic of LED (a) LED chip (b) LED lamp

Since the photons will be incident upon the chip walls, we apply basic principles of optics to analyze the phenomenon when light travels from one medium into another. According to the boundary condition shown in Figure 4.2, the transmittance and reflection coefficients at the arbitrary angle are given by [22]

$$\Gamma_{TE} = \frac{n_s \cos \theta_i - n_e \cos \theta_t}{n_s \cos \theta_i + n_e \cos \theta_t}$$
$$\Gamma_{TM} = \frac{n_s \cos \theta_t - n_e \cos \theta_i}{n_s \cos \theta_i + n_e \cos \theta_t}$$

$$T_{TE} = 1 - |\Gamma_{TE}|^2$$

$$T_{TM} = 1 - |\Gamma_{TM}|^2$$

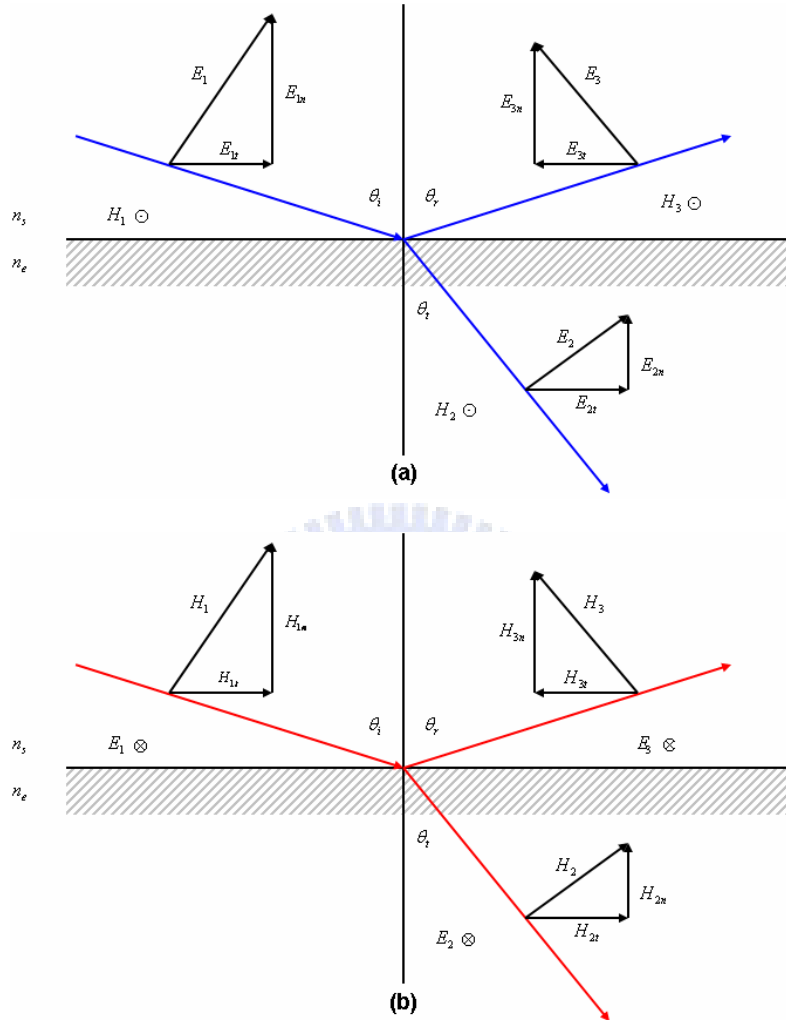


Fig 4.2 Boundary condition at the interface between two media. (a) TM (b) TE

where n_s and n_e are the refractive index of the chip and the encapsulant epoxy, respectively, and θ_i and θ_t are the incidence and transmission angles, respectively. The relation between θ_i and θ_t can be obtained from Snell's law, and the critical angle is expressed as

$$\theta_c = \sin^{-1}(n_e / n_s)$$

Figure 4.3 shows the transmittance as a function of the incidence angle. Note that the transmittance of TM polarization is always greater than that of TE polarization. The

sharp window between $-\theta_c$ to θ_c leads to the so-called extraction cone.

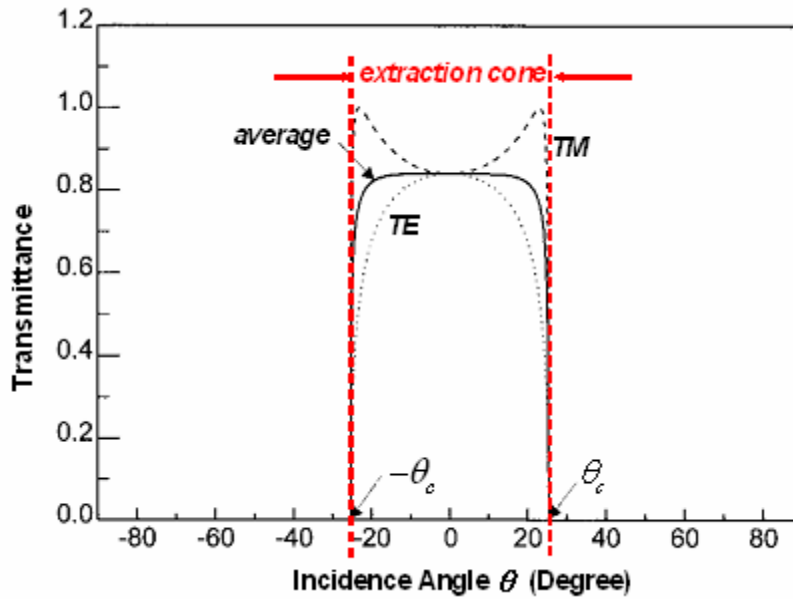


Fig. 4.3 Transmittance as a function of incident angle θ_i

The solid angle of extraction cone for each facet of the chip can be expressed by (assuming that refractive-index among layers are relatively small)

$$\Omega_c = \int_{\phi=0}^{2\pi} \int_{\theta=0}^{\theta_c} \sin \theta d\theta d\phi = 2\pi \{1 - [1 - (\frac{n_e}{n_s})^2]^{1/2}\}$$

The photons emitted with an angle larger than θ_c would undergo TIR and would be trapped inside the chip, as illustrated in Fig. 4.3.

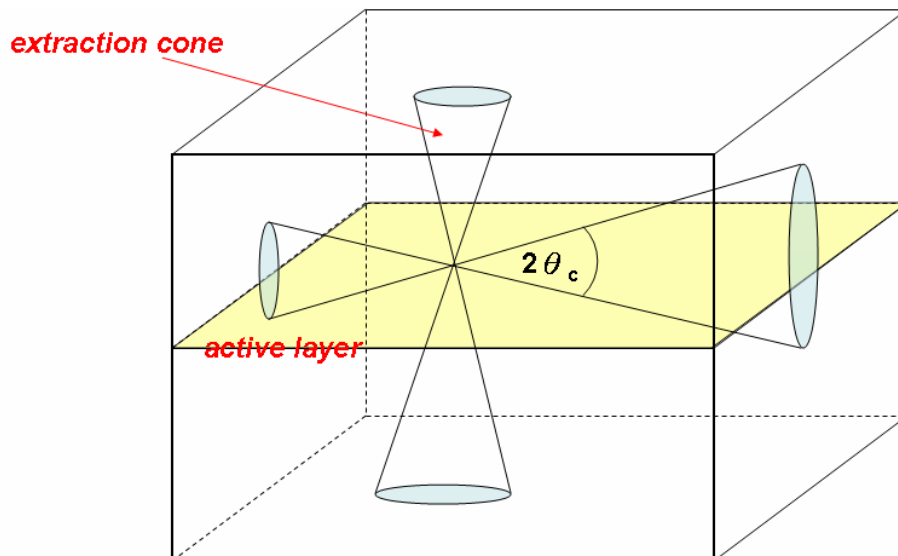
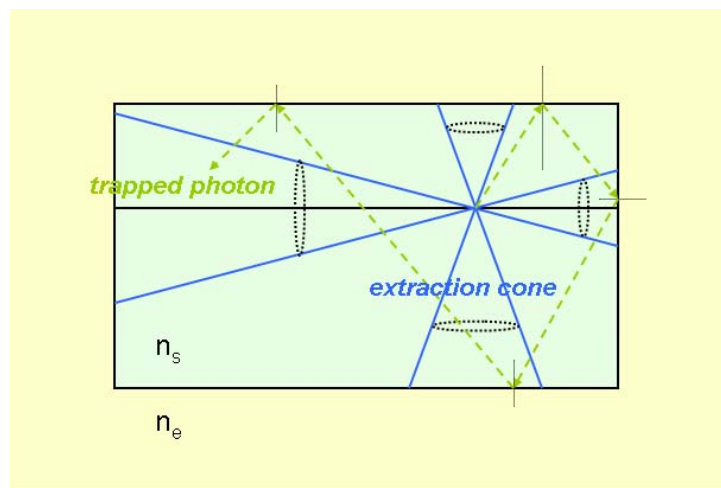


Fig 4.4 Escape cone of a photon at active layer

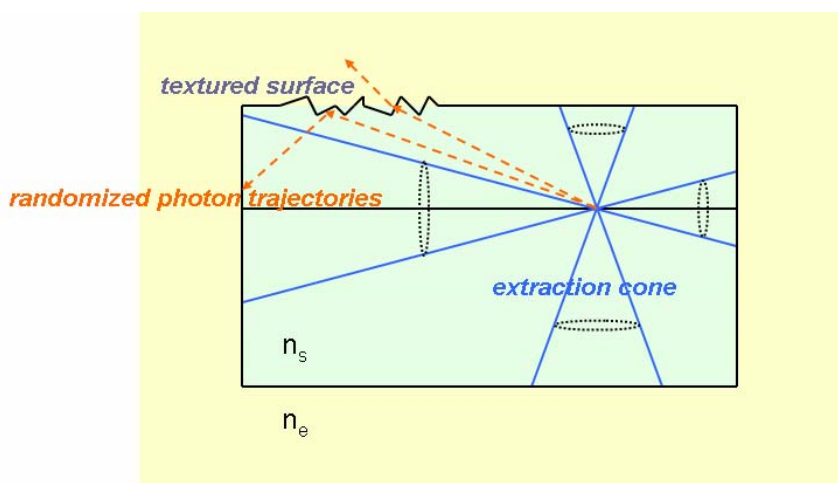
The fraction of the trapped photons can be expressed approximately as [23]

$$\eta_{trap} = \frac{4\pi - 6\Omega_c}{4\pi} = 3\left[1 - \left(\frac{n_e}{n_s}\right)^2\right]^{1/2} - 2$$

With $n_e=1.5$ and $n_s=3.5$, around 71% of total emitted photons would be trapped and absorbed eventually. The external quantum efficiency is seriously limited due to such a large fraction of trapped photons. A method to extract the photons confined in the substrate due to TIR is texturing the surface, as illustrated in Figure 4.5 (b). The photons incident upon the textured surface will undergo photon trajectory randomization and will have some chance to be coupled out of the chip.



(a)



(b)

Fig 4.5 (a) trapped-photon trajectories in flat surface chip (b) randomized photon trajectories off a textured surface

Even though the concept of extraction cone provides a general idea for the photon coupled out process, it encounters limitations when seeking reliable result of analyzing LED with complex shaped surface.

4.2 Introduction to Monte Carlo method

In LED's, the photons are generated in the active region with random directions. The probability of photons to be coupled out of device depends on their directions of emission. As a result, the analysis of LED may not be an easy task compared with laser diode since in which most of the photons travel along a direction that is well defined by the cavity mode [23].

Conventionally, LED's are analyzed by extraction cone methods [23]. However, this method is limited to qualitative analysis. Furthermore, serious limitations are encountered when analyzing LED's with complicated geometry. Monte Carlo photon-simulation overcomes the limitations of extraction cone method and is applicable to any chip geometry. The unique versatility of Monte Carlo makes it easy to analyzing or designing LED's. Basically, Monte Carlo photon-simulation is based on statistical tracing of photons and the simulation result is quite realistic. In addition, the method can incorporate complex photon-propagation models relatively easily.

Generally speaking, the effect of feedback of by the facets of the chip is negligible. Therefore, most of the photons generated in the active region are spontaneous emission and incoherent. (The incoherent photons can be treated as particles instead of as waves) The spontaneously emitted incoherent photons take free flights in random directions until interrupting by various flight-disrupting events, such as scattering, absorption, photon recycling, or reflection/refraction at the interfaces among layers.

An optical simulation and analysis program, Advanced System Analysis Program

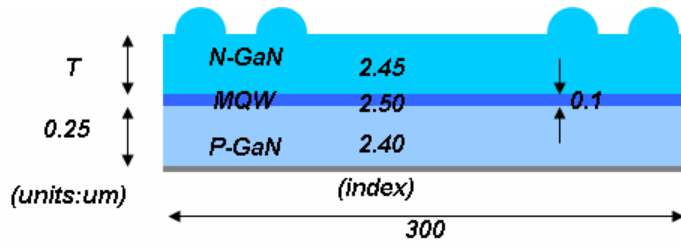
(ASAP), was used to simulate the microlens-based LED by Monte Carlo ray-tracing. In our simulation, only the effect of absorption by material and Fresnel reflection at interface are considered.

4.3 Microlens array based LED

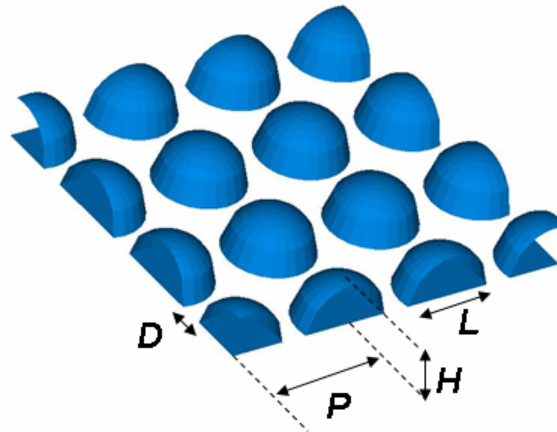
A drawback of both OLED and LED is that only small fraction of the emitted light can escape into air owing to total internal reflection (TIR) in the high refractive index substrate. Light extracted outside of device with a narrow escape cone suffers TIR as well as waveguiding. Hence, almost 80% of the generated light is lost due to TIR and waveguiding [25~27]. Methods employed to overcome efficiency limitations due to light trapping concentrate on expanding the escape cone of the substrate and suppressing the waveguide modes. Although a significant increase of η_{ext} was observed for the reported approaches, they are often accompanied by changes in the radiation pattern, exhibit an undesirable angle dependent emission spectrum, or employ costly or complex fabrication process [8].

Here in this chapter, we demonstrate an enhancement of the extraction efficiency by utilizing an ordered microlens array. The optical properties of the lens sheets are modeled by ray-tracing calculation.

As depicted in Figure 4.6 (a), the ordered microlens array is placed on the top of the surface to reduce the effect of TIR. By means of microlens array, escape cone can be expanded which would cause more light extracted into air. To optimize the efficiency of microlens-based LED/OLED, some parameters are considered, such as the geometric shape of lens, the period P (filling factor F), and the thickness between lens bottom to the source position T, as denoted in Figure 4.6 (b).



(a)



(b)

Fig. 4.6 (a) Optical model of LED with microlens array (b) parameters of microlens array

For simplicity, the metal cathode is assumed to be an ideal reflector. Microcavity effects and the waveguiding are not considered since the microlenses do not significantly affect these processes [8]. Light generated in the emitting layer is traced through the devices considering Fresnel reflection at interfaces between layers with different refractive indices.

Rays that approach the flat top surface with an incident angle larger than the critical angle suffer TIR. As the surface coated with microlens array, however, the angle of incidence can be smaller than critical angle which leading to extraction of light.

4.3.1 Mathematical prediction

The following simulation of microlens array on LED is accomplished by adopting ray-tracing method. Since the ray-tracing method is based on the consideration of refraction and reflection at the media interfaces, a mathematical calculation by Snell's law is performed in advanced.

Some assumptions are made for simplicity. The light/photons emitted from the active region is modeled as an isotropic source. According to the weak form of radiance theorem, after propagating a certain distance (thickness of GaN), the light distribution detected on the bottom of the lens should be randomly distributed as well, as shown in Figure 4.7. This assumption stands only for the microlenses located in the central region. The light detected on the bottom of lenses located at the corner of LED would be affected by the light reflected from the wall of LED. Therefore, the light distribution detected at the edge may not have the same as those in the central part.

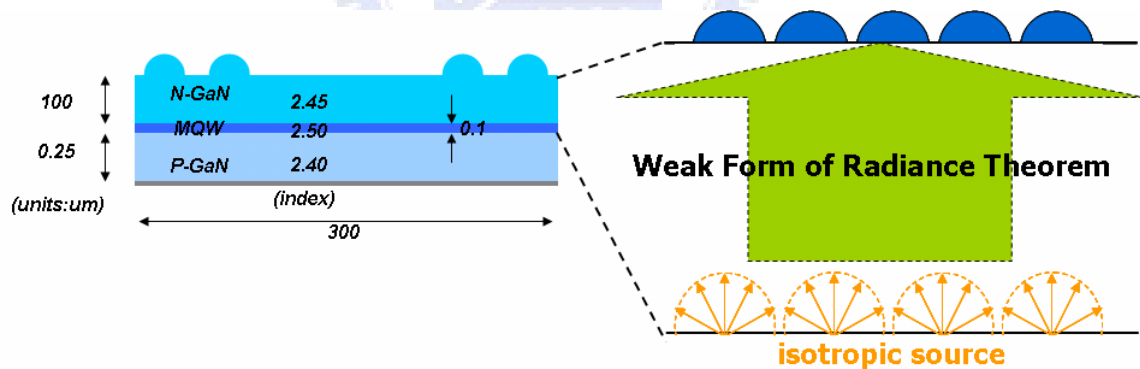


Fig. 4.7 The light distribution in the active region and bottom of central microlens.

The following calculation is based on the assumption made above. Each point at the bottom of lens is regarded as point sources. In Figure 4.8 (a), the relative solid angle of extraction cone at each point is estimated. For instance, θ_2 is the relative solid angle at the point 2. The relative angles are summed from point 1 to point 3 because of the symmetry of lens. The relation between H, R and L can be simply

derived as followed.

$$R = \frac{H^2 + (L/2)^2}{2H}$$

Under the same diameter of lens (L), we calculate Θ_{All} with different curvatures. H is varied from 0 to (L/2). Θ_{All} is regarded as an index of the lens extraction.

$$\Theta_{All} = \sum_i \theta_i$$

The calculation result is shown in Figure 4.8 (c).

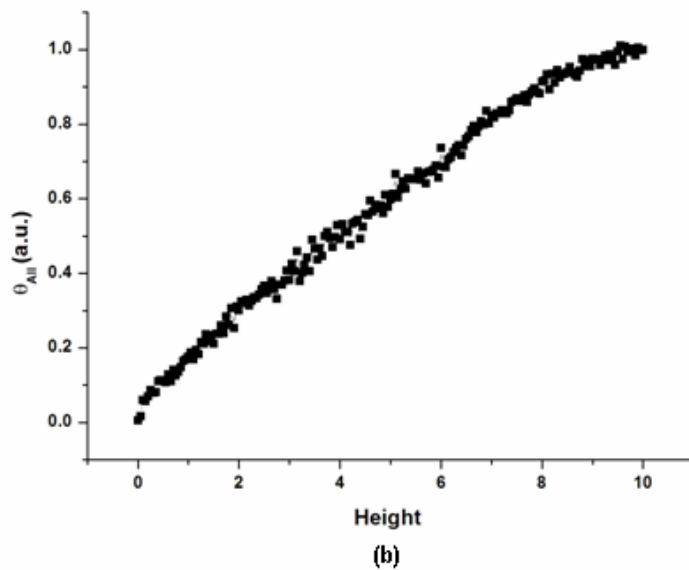
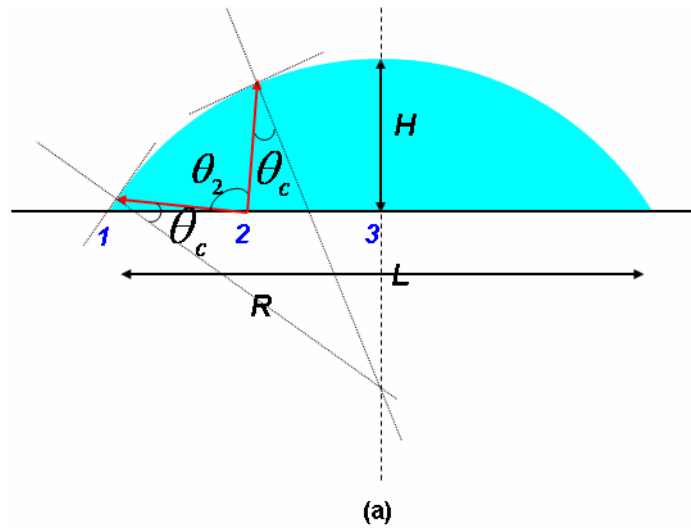


Fig 4.8 Illustration of calculating (a) Θ_{All} (b) calculation result

4.3.2 Ray-tracing simulation result

The mathematical prediction obtained above is not applicable to the realistic case since the assumption is valid only for the lens located in the central part. Moreover, the absorption of material and the light reflection/guided inside substrate (GaN) are not considered which would result in serious discrepancy of simulation result. Therefore, with the aid of optical simulation program, more reliable and efficient simulation result can be obtained.

We applied the optical model shown in Figure 4.6 (a) to ASAP for obtaining the extraction efficiency with different heights (H) of lenses. The distance between adjacent lens is set to $1\mu\text{m}$ and the diameters of lenses are 5, 10, 15 and 20 μm (L5, L10, L15, L20), respectively. As shown in Figure 4.9, the trend of the simulation curves have similar tendency to that of the mathematical predicted curve. The enhancement factor (E.F.) increases as the height of the lens becomes larger. The E.F. reaches to the highest value when the height is $L/2$. In other words, microlens array with hemisphere shape couples the most substrate-guided light. Moreover, higher enhancement can be obtained by increasing the filling factor.

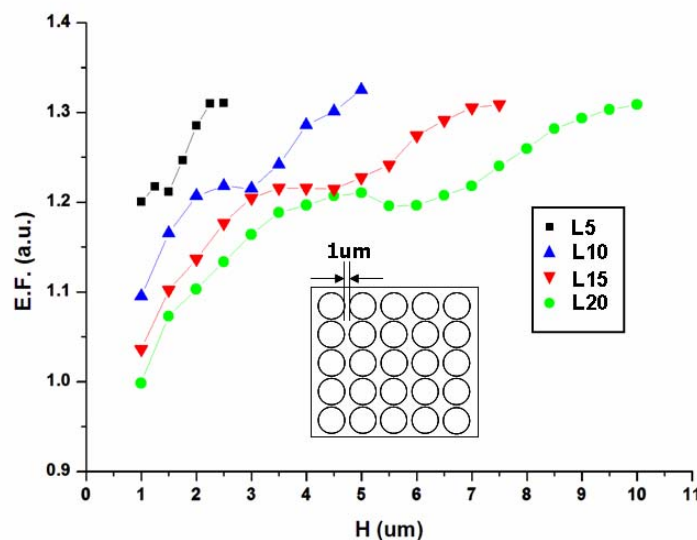


Fig 4.9 Enhancement factor with different L and H

Next we consider the influence of filling factor on the enhancement factor. Figure 4.10 shows the E.F. of different filling factors. The diameter of microlens array is all set to be 10 μm with different filling factors. The filling factor is regarded as the area influenced by microlens array. As expected, E.F. decreases as filling factor becomes lower.

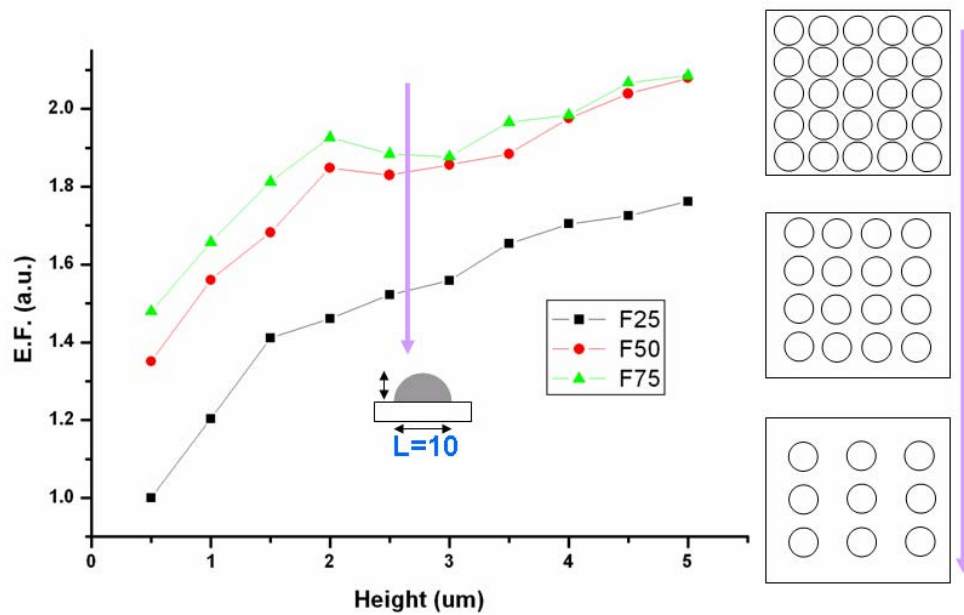


Fig. 4.10 Enhancement factor with different filling factors.

For the microlens array with the geometric shape beyond hemisphere (called superlens) is also considered. Preventing the adjacent lenses from touching each other, the filling factor for considering the influence of superlens is set to be 50%.

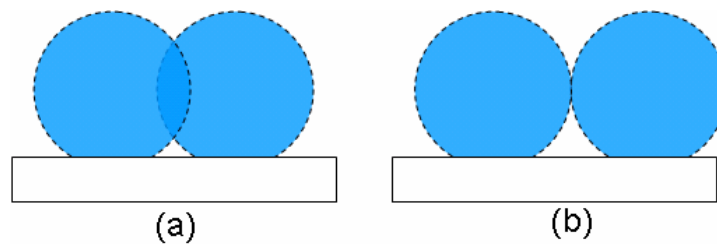


Fig. 4.11 Filling factor (a) $>50\%$ (b) 50%

The bottom of the superlens is 10 μm in diameter with the filling factor 50%. The height is now defined as the distance from center of a superlens to the LED surface. Despite of the shape of superlens, the light distribution detected at the bottom area should be the same. Whether the light at the bottom can be extracted into air depends on the superlens shape. According to the simulation result, we can come to a conclusion that the lower the height of the superlens is, the higher the E.F. becomes. Higher superlens may result in more light confined inside the superlens instead of extracting light into air. As a result, E.F. decreases as the height becomes larger as shown in Figure 4.12. This result may be due to the curvature of superlens as well. Since the light emitted into superlens are the same (because of same bottom area), it seems that the superlens with smaller curvature results in higher E.F..

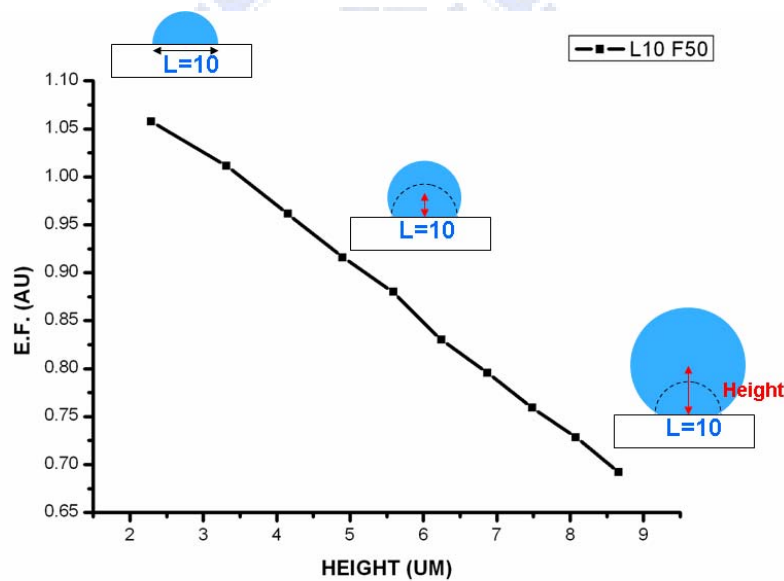


Fig. 4.12 E.F. with different heights of superlens

Next we consider the microlens array with the same curvature with different bottom areas. Under the same curvature, the microlens array with higher coverage ratio results in higher E.F.. The simulation result is shown in Figure 4.13.

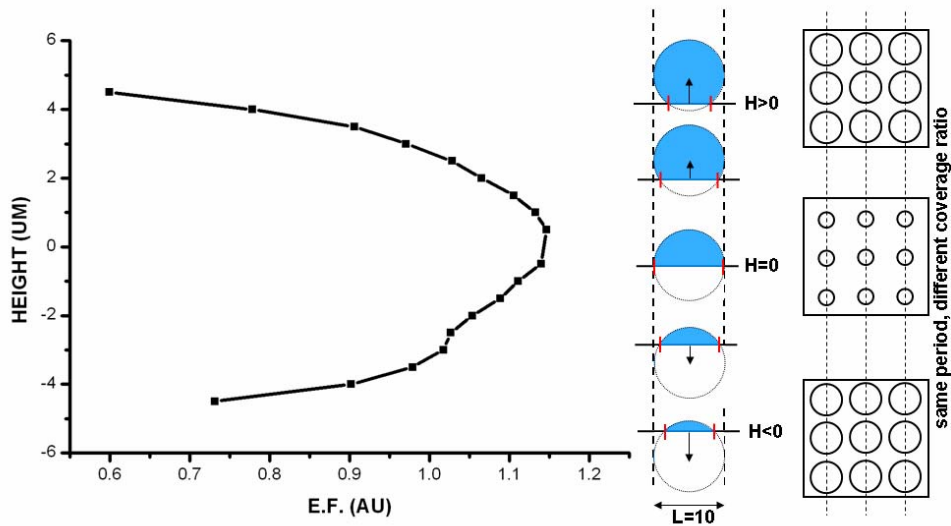


Fig. 4.13 E.F with different coverage ratio under the same curvature.

From the simulation results shown in Figure 4.12 and Figure 4. 13, we can make a brief conclusion about the influence of lens curvature and coverage ratio illustrated in Figure 4.14.

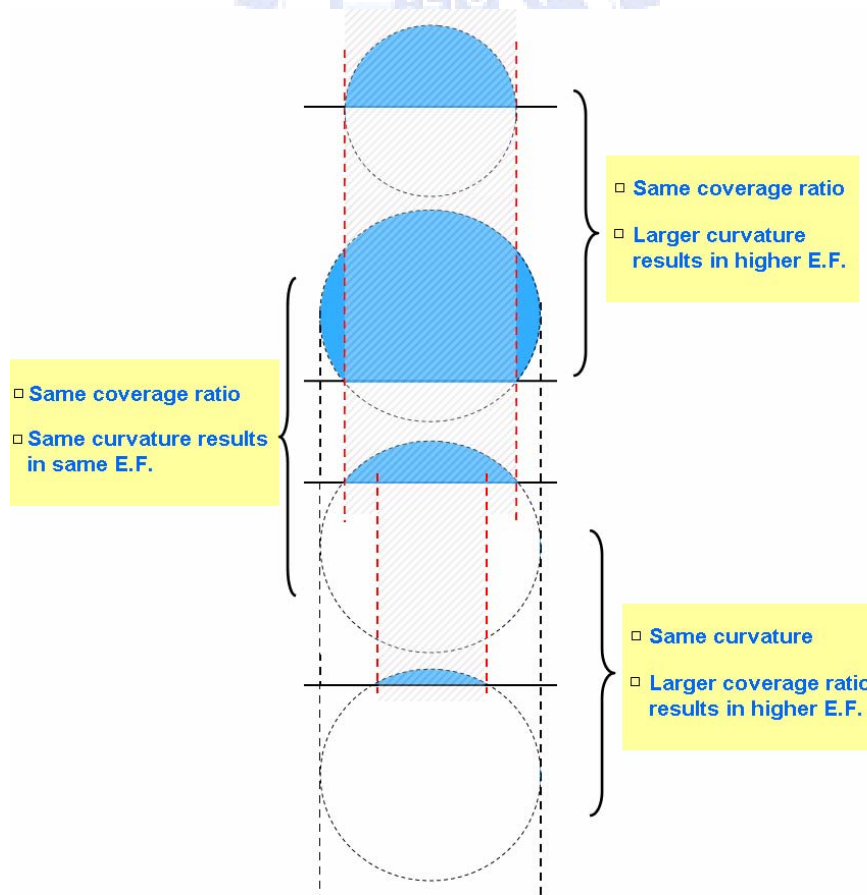


Fig. 4.14 Illustration of relation between E.F. and (1) coverage ratio (2) curvature

Chapter 5

Conclusion

Electroluminescent devices such as OLEDs or LEDs become more and more important and play a crucial role in the next generation display and illumination applications. However, as addressed previously, the low light extraction efficiency is still one of the key issues needed to be solved if one wants to apply the OLEDs/LEDs devices as the lighting sources. Several approaches have been proposed to increase the light extraction efficiency. We focus our research on optical structures for enhancing the efficiency. Here in this thesis, the utilizations of photonic crystal (PC) and micro-lens array applied on OLED and LED are presented and demonstrated. By using nano (PC) and micro (microlens array) scale optical structures, the light extraction efficiency of OLEDs/LEDs can be improved.

As shown in Figure 2.1(a) (structure) and Figure 2.14 (result), based on our simulation result when applying the photonic crystal into OLED 117% of the light extraction efficiency can be enhanced. Higher enhancement is expected if the refractive index difference of photonic crystal can be increased. In our model, only 0.34 of the refractive index difference is achieved. ($\text{SiN}_x=1.8$, UV glue=1.46) Limited to the fabrication process, the refractive index of SiN_x is only 1.8. According to the spec, the refractive index of SiN_x should be larger than 2. However, as mentioned above, this poor feature is because of the limitation of fabrication process. Better quality of refractive index of SiN_x can be achieved if the fabrication process can be improved.

As for the application of microlens array on LED, hemisphere shape of microlens array enhances the most of light extraction efficiency. 1.35X of

enhancement can be achieved if the filling factor is 100% and the shape of microlens array is hemisphere.



Reference

- [1] S.R. Forrest, D. D. C. Bradey and M. E. Thompson: *Adv. Mater.* 15, 1043 (2003)
- [2] M. Fujita, k. Ishihara, T. Ueno, T. Asano, S. Noda, H. Ohata, T. Tsuji, H. Nakada and N. Shimoji, *Jpn. J. Appl. Phys.*, Vol. 44, No. 6A, P. 3669-3677 (2005)
- [3] L. S. Hung, L. R. Zeng, and M. G. Mason, *Appl. Phys. Lett.* 78, 673 (2001)
- [4] K. Murata, S. Cina, and N. Greenham, *Appl. Phys. Lett.* 79, 1193 (2001)
- [5] L. S. Hung, C. W. Tang, and M. G. Mason, *Appl. Phys. Lett.* 70, 152 (1997)
- [6] Y. R. Do, Y. C. Kim, Y. W. Song, and Y. H. Lee, *J. Appl. Phys.*, Vol. 96, No. 12 (2004)
- [7] M. Boroditsky, T. F. Krauss, R. Coccioli, R. Vrijen, R. Bhat, and E. Yablonovitch, *Appl. Phys. Lett.* 75, 1036 (1999)
- [8] S. Möller and S. R. Forrest, *J. Appl. Phys.*, Vol. 91, No. 5 (2002)
- [9] H. Peng, Y. L. Ho, X. J. Yu, M. Wong, H. S. Kwok, *J. Display Tech.*, Vol. 1, No. 2 (2005)
- [10] Y. J. Lee, S. H. Kim, J. Huh, G. H. Kim, Y. H. Lee, S. H. Cho, Y. C. Kim and Y. R. Do, *Appl. Phys. Lett.*, Vol. 82, No. 21 (2003)
- [11] Y. J. Lee, S. H. Kim, G. H. Kim, Y. H. Lee, S. H. Cho, Y. W. Song, Y. C. Kim and Y. R. Do, *Opt. Exp.*, Vol. 13, No. 15 (2005)
- [12] D. Delbeke, P. Bienstman, R. Bockstaele and R. Baets, *J. Opt. Soc. Am. A*, Vol. 19, No. 5 (2002)
- [13] J. H. Lee, K. Y. Chen, C. C. Hsiao, H. C. Chen, C. H. Chang, Y. W. Kiang and C. C. Yang, *J. Disp. Tech.*, Vol. 2, No. 2 (2006)
- [14] W. Lukosz, *J. Opt. Soc. Am.* Vol. 67, No. 12, (1977)
- [15] R. Zengerle, *J. Mod. Opt.* Vol. 34, No. 12, P. 1589-1617 (1987)
- [16] H. Rigneault, F. Lemarchand and A. Sentenac, *J. Opt. Soc. Am. A*, Vol. 17, No. 6 (2000),
- [17] H. Rigneault, F. Lemarchand, A. Sentenac and H. Giovannini, *Opt. Lett.*, Vol. 24, No. 3 (1999)
- [18] J. D. Joannopoulos, R. D. Meade, J. N. Winn, Princeton Univ. Press.
- [19] A. Chutinan, k. Ishihara, T. Asano, M. Fujita, S. Noda, *Org. Elec.* 6, P. 3-9 (2005)
- [20] L. Jay Guo, *J. Phys. D: Appl. Phys.* 37 R123-R141 (2004)
- [21] B. Michel, A. Bernard, A. Bietsch, E. Delamarche, M. Geissler, D. Juncker, H. Kind, J. P. Renault, H. Rothuizen, H. Schmid, P. Schmidt-Winkel, R. Stutz and H. Wolf, *IBM J. Res. & Dev.*, Vol. 45, No. 5 (2001)
- [22] Keigo Iizuka, *Wisley-interscience*, Volume I
- [23] S. J. Lee, *Appl. Opt.*, Vol. 40, No. 9 (2001)
- [24] V. Bulovic, V. B. Khalfin, G. Gu, P. E. Burrows, D. Z. Garbuzov, and S. R.

- Forrest, Phys. Rev. B 58,3730 (1998)
- [25] Schubert, E. Fred, Cambridge Univ. Press (2003)
- [26] T. X. Lee, C. Y. Lin, S. H. Ma and C. C. Sun, Opt. Exp., Vol. 13, No. 11 (2005)
- [27] M. K. Wei and I. L. Su, Opt. Exp., Vol. 12, No. 23 (2004)

